

https://dspace.org/

Estimating urban greenness index in the city of Johannesburg: a case study of Soweto vs Rosebank suburbs

Mudede, Marko Freddy

2019
https://hdl.handle.net/10539/28864

Downloaded from a DSpace repository. https://dspace.org/



MSc Report

Estimating urban greenness index in the city of Johannesburg: a case study of Soweto vs. Rosebank suburbs.

Marko Freddy Mudede

(1803163)

Supervisor: Dr Solomon Newete

Co-Supervisors: Dr Khaled Abutaleb

Prof Nsalambi Nkongolo

A research report submitted in partial fulfillment of the requirements for the degree of Master of Science

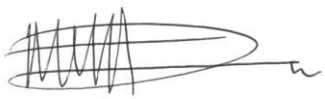
University of the Witwatersrand

School of Animal, Plant and Environmental Sciences

May 2019

DECLARATION

I, Marko Freddy Mudede, declare that this work is my own. It is being submitted for the research report component of the Degree of Master of Science at the University of the Witwatersrand, Johannesburg. It has not been submitted before for any degree or examination at any other University.



Signature …… … **Date …29…. May……2019……**

DEDICATION

This research is dedicated to my parents, Mr. B.T.W. Mudede and Mrs. E. Mudede.

ACKNOWLEDGEMENTS

Firstly, special thanks go to my academic supervisors Dr. Solomon Newete, Dr. Khaled Abutaleb and Prof. Nsalambi for their guidance, technical and field work assistance and for making this research project a success, without their support I would not have reached this far. Also, the support I received from my family and relatives is greatly appreciated throughout the hard times at Wits and it was not an easy task to complete my studies.

I wish to thank the following; Dr. Khaled Abutaleb for assisting me during data analysis and all the technical aspects of the research; Dr. Solomon Newete for reading and providing useful criticism of the research project. I would like to extend my special gratitude to Wits School of Governance (WSG) at the University of the Witwatersrand for all the financial support of my research field expenses through the 'Life in City" project (Project #: 2858) lead by Dr S. Newete; the South African National Space Agency (SANSA) team for SPOT 6 satellite images of Rosebank and Soweto suburbs; United States Geological Survey (USGS) for free access to Landsat 8 satellite images; R core team for use of their R software for random forest classification; Mr. A. Bello for allowing me to use his laptop during data analysis; Faith, Solange and Mphako for all the support and encouragement during my stay at Wits.

Lastly, I would like to thank the Zimbabwe Government and National Scholarships Department and the Executive Director Dr. C.C. Mushohwe for making this academic journey a success by granting me a scholarship to further my studies at the University of Witwatersrand. Also, I wish to thank the whole team at the scholarship department for all the necessary help and assistance whenever needed.

Above all, I give thanks and praises to the Almighty, Jesus Christ who gives me guidance and strength.

ABSTRACT

Urban greenness plays a significant role in providing ecosystem services and disservices which directly affects the health status of urban city's dwellers. Factors like impervious concrete surfaces or tarred roads and tree cover contribute to changes in urban land surface temperature. The change in urban temperatures will result in differing local temperatures compared to surrounding areas leading to urban heat island effect. Urban greenness index in the city of Johannesburg of South Africa was investigated in Soweto and Rosebank suburbs to determine its environmental suitability for its inhabitants. A total of 120 street tree species composed of *Jacaranda mimosifolia* and *Platanus acerifolia* were recorded, and GPS points from each of these trees were collected from Rosebank for ground-truthing. In this study two satellite images of Landsat 8 and SPOT 6 were used for analysis. Landsat 8 data was used to evaluate the effects of urban heat island phenomenon based on urban thermal field variance and ultraviolet indices. Soweto had the highest total biomass of 504399.97 tons while that of Rosebank was 113179.03 tons. However, Rosebank suburb had a higher greenness index value of 0.82 compared to that of Soweto (0.14) and this gives a clear pattern of the ecological disparity between the two areas. The Land Surface Temperature (LST) of Soweto showed a higher value (2.58 ^{o}C more) compared to that of Rosebank suggesting that high-density areas are hotter than low-density suburbs. Pearson correlation coefficient was performed among NDVI, LST and Normalized Difference Built-up Index (NDBI) and a confusion matrix were derived. The results showed a positive correlation between LST and NDBI (0.92 and 0.98) and a negative correlation between LST and NDVI (-0.91 and -0.99) and NDVI vs. NBDI (-0.90 and -0.85) in Rosebank and Soweto areas. Based on urban thermal field variance (UTFVI) analysis, it shows that residents of Soweto face more thermal discomfort compared to residents of Rosebank suburb. Similarly, analysis of the global solar ultraviolet index (UVI) indicated that Soweto residents' life is more vulnerable to prolonged exposure to ultraviolet solar radiation than those in Rosebank. Overall, land surface temperature for the two study areas was successfully retrieved from Landsat 8 data and the information obtained from this study will provide a baseline for future planning on improving the greenness of urban cities.

Keywords: Urban greenness; Above Ground Biomass; Remote Sensing; Urban Heat Island, Land Surface Temperature; Urban Thermal Field Variance and Solar Ultraviolet Index; *Jacaranda mimosifolia*; *Platanus acerifolia*

TABLE OF CONTENTS

DECLARATION i
DEDICATION ii
ACKNOWLEDGEMENTS iii
ABSTRACT iv
LIST OF TABLES vii
LIST OF FIGURES viii
LIST OF ABBREVIATIONS ix
CHAPTER 1: INTRODUCTION 1
1.1 Background 1
1.2. Rationale 3
1.3. Research questions 4
1.4. Problem statement 4
1.5. Aim and objectives 5
CHAPTER 2: LITERATURE REVIEW 7
2.1. History of urban greenness in the city of Johannesburg 7
2.2. Importance of urban greenness 7
2.3. Plant biomass estimation using nondestructive methods 8
2.4. Estimating plant biomass using remote sensing 9
2.5. Vegetation indices 10
2.6. Urban heat island 11
CHAPTER 3: METHODOLOGY 13
3.1. Description of the study areas 13
3.2. Experimental design 15
3.3. Biomass estimation 15
3.3.1. Field biomass estimation using the allometric equations 15
3.3.2. Extraction of AGB from SPOT 6 satellite images 16
3.4. Field data collection 17
3.5. Remote Sensing Data 18
3.6. Image acquisition and processing 18
3.7. Image classification 18
3.7.1. Random Forest classification 19
3.8. Vegetation index 21
3.9. Urban heat island 22

3.9.1. Top of Atmospheric (TOA) spectral radiance calculation 25
3.9.2. Conversion of TOA to BT 25
3.9.3. Converting BT from Kelvin to degrees Celsius 26
3.9.4. Normalized Difference Vegetation Index (NDVI) calculation 26
3.9.5. Calculation of the proportion of vegetation (P_v) 26
3.9.6. Calculation of Land surface emissivity (ε) 27
3.9.7. Calculation of Land surface temperature 27
3.10. Normalized Difference Built-up Index (NDBI) calculation 28
3.11. Surface radiation estimation 28
3.12. The Urban Thermal Field Variance Index (UTFVI) 29
3.13. Statistical Analysis 30
CHAPTER 4: RESULTS 32
4.1. Plant biomass estimation using allometric equation and remote sensing 32
4.1.1. Random forest classification 35
4.1.2. Accuracy assessment 35
4.2. Vegetation index 37
4.3. Urban heat island 38
CHAPTER 5: DISCUSSION AND CONCLUSIONS 45
5.1. Biomass estimation and remote sensing 45
5.2 Greenness Index 46
5.3. Urban heat island 46
5.4. Conclusions 50
5.5. Recommendations 51
REFERENCES 52
APPENDICES 61

LIST OF TABLES

Table 3.1: Land cover classes of Rosebank and Soweto suburbs in Johannesburg selected for Random Forest classification. 19

Table 3.2: Description of Normalized difference vegetation index (NDVI) classes for Rosebank and Soweto suburbs 22

Table 3.3: Landsat 8 image metadata file downloaded for the city of Johannesburg (Rosebank and Soweto) for the calculation of brightness temperature (BT) and top of atmospheric (TOA). 25

Table 3.4: Description of Land surface temperature (LST) classes for Rosebank and Soweto areas in Johannesburg. 28

Table 3.5: The Global solar ultraviolet (UV) Index threshold used for solar radiation classification for Rosebank and Soweto areas. 29

Table 3.6: Ecological evaluation index threshold values for classifying urban heat island phenomenon in Rosebank and Soweto areas in Johannesburg. 30

Table 4.1: Carbon content in above ground biomass (AGB) and greenness index of Rosebank and Soweto suburbs in Johannesburg. 33

Table 4.2: Results of Random Forest classification of land cover classes of Rosebank and Soweto areas in Johannesburg. 35

Table 4.3: Confusion matrix for Rosebank obtained from Random Forest classifier. 36

Table 4.4: Land surface temperature (LST) results of Rosebank and Soweto suburbs in Johannesburg derived from Landsat 8 data. 40

Table 4.5: Results of Pearson correlation coefficient among Normalized Difference Built-up Index (NDBI), Normalized Difference Vegetation Index (NDVI) and Land Surface Temperature (LST) of Rosebank and Soweto suburbs in Johannesburg. 41

Table 4.6: Results of Urban Thermal Field Variance Index (UTFVI) coverage in Rosebank and Soweto suburbs in Johannesburg derived from Landsat 8 data. 42

Table 4.7: Results of global solar Ultraviolet (UV) index analysis for Rosebank and Soweto suburbs in the city of Johannesburg. 44

LIST OF FIGURES

Figure 3.1: Location of study areas of Rosebank and Soweto suburbs in Johannesburg. 14
Figure 3.2: Flow chart diagram showing steps of SPOT 6 image analysis. 20
Figure 3.3: Flow chart diagram for land surface temperature (LST) calculation using Landsat 8 data. 24
Figure 4.1: Correlation relationship between estimated above ground biomass and normalized difference vegetation index (NDVI). 33
Figure 4.2: Maps of above ground biomass for (a) Rosebank and (b) Soweto areas in the City of Johannesburg derived from SPOT 6 satellite image. N.B. Dark green- high biomass, yellow- medium biomass, grey- low biomass, white- no biomass. 34
Figure 4.3: Maps of carbon content sequestered in plant biomass for (a) Rosebank and (b) Soweto areas in the City of Johannesburg. N.B. Dark green- high carbon, yellow- medium carbon, grey- low carbon, white- no carbon. 34
Figure 4.4: Classified SPOT 6 pan-sharpened images for land cover classes of (a) Rosebank and (b) Soweto, in Johannesburg. 37
Figure 4.5: Normalized Difference Vegetation Index (NDVI) classification maps of Rosebank (a) and Soweto (b) areas, in Johannesburg derived from SPOT 6 data. 38
Figure 4.6: Land surface temperature maps of Rosebank (a) and Soweto (b) suburbs obtained from Landsat 8 data. 39
Figure 4.7: The maps of Normalized Difference Built-up Index of (a) Rosebank and (b) Soweto suburbs derived from Landsat 8 satellite data. 41
Figure 4.8: Ecological assessment of (a) Rosebank and (b) Soweto suburbs based on Urban Thermal Field Variance Index (UTFVI) in the City of Johannesburg. 43
Figure 4.9: Maps showing extend of solar radiation exposure estimated from Global Solar Ultraviolet (UV) index in the suburbs of Johannesburg (a) Rosebank and (b) Soweto. 44

LIST OF ABBREVIATIONS

AGB- Above Ground Biomass

ENVI - Environment for Visualising Image

FLAASH - Fast Line of Sight Atmospheric Analysis of Spectral Hypercubes

GIS - geographic information system

GPS - global position system

LST - Land surface temperature

MTL - Material library files

NDVI - normalized difference vegetation index

RF - random forest

RS - remote sensing

SANSA - South African National Space Agency

SOWETO - South Western Townships

SPOT - Satellite Pour I' Observation de la Terre

UHI - Urban Heat Island

USGS - United States Geological Survey

UTFVI - Urban Thermal Field Variance Index

UTM - Universal Transverse Mercator

UVI - Ultraviolet Index

VI - Vegetation index

WGS -World Geodetic System

CHAPTER 1: INTRODUCTION

1.1 Background

Urban greenness is becoming an important aspect or constituent of the urban environment through various services that contribute to the general health quality of citizens and minimizing the effects of extreme weather conditions and air pollution. A survey by the World Health Organization (2013) showed that 50 % of the global population lives in an urban environment and this figure is expected to increase by 10 % by 2050. Urban greenness refers to places with natural surfaces or natural settings including street trees, open space (water elements), riverside footpaths, although the definition is context specific depending on the environment under consideration (WHO, 2016). Population growth and urbanization have contributed to changes in the quality and quantity of urban greenness (Tan *et al*., 2013). The rising urban expansions are often responsible for degrading the existing greenness in urban centres and urban fringes.

The urban vegetation may include native and exotic tree species. Most of the urban trees in many developing countries, predominantly in Sub-Saharan Africa are the legacy of the European colonist and as such, they are predominantly alien trees (Turton *et al*., 2006). *Eucalyptus* and *Acacia* (e.g. black wattles) trees were among the prominent species imported from Australia either for suppression of sand dunes or for phytoremediation and mining props in mining areas in Johannesburg (Newete *et al*., 2011). However, later this plant (*Eucalyptus*) became a major threat to water resource in South Africa, (Turton *et al*., 2006). *Eucalyptuses* are known for high water consumption and they drain ground waters through their unprecedented evapotranspiration abilities (Turton *et al*., 2006). Elsewhere, in the city of Kigali (Rwanda) more than 75 % of the urban trees are exotics originally from Tropical Asia, Tropical America and Australia (Seburanga *et al*., 2014). Some of the trees include *Jacaranda mimosifolia*, *Eucalyptus* spp and *Cassia spectabilis* and they are most dominant in roadside (Seburanga *et al*., 2014).

Evaluating urban greenness by mapping tree biomass using remote sensing is important for planning and management purposes of urban environments. Plant biomass estimation in urban areas gives an indication of the ecological status for better city planning and management of vegetation. Tree biomass of an area can be estimated using field measurements (Brown *et al*., 1989; Dudley and Fownes, 1992; Tietema, 1993; Gibbs *et al*.,

2007), geographic information system and remote sensing methods (Lu, 2005). The traditional field method of estimating biomass involves measuring structural attributes for individual tree species and uses allometric equations to calculate biomass (Nowak, 1993; Sousa *et al*., 2015). Plant biomass can be estimated using both destructive (Vashum and Jayakumur, 2012; Ngo and Lum, 2018) and non-destructive sampling methods (Lu, 2006). The destructive method is expensive, resource wasteful and labour intensive (McHale *et al*., 2009). Thus, this destructive method could be replaced by a remote sensing technique to map and estimate urban green biomass at large scale effectively. The destructive method involves cutting down trees and measuring the weight of tree trunk, branches and leaves followed by oven drying (Vashum and Jayakumur, 2012). A nondestructive method does not involve tree felling since data is acquired using remote sensing technique (Xie *et al*., 2008) and allometric equations (Nowak, 1993) for plant biomass estimation. Two types of basic allometric equations are 'general' and 'species-specific' equations. In this research, remote sensing technique and species-specific equations were used to estimate plant biomass. Estimating plant biomass using allometric equation is cheap and requires less labour (Vashum and Jayakumur, 2012). Remote sensing technology enables the easy acquisition of information about objects without any geographical barriers of accessibility.

The application of remote sensing technique in mapping plant biomass has shown an unprecedented increase in recent years. The surge is attributed to the availability of a variety of medium and high-resolution satellite imageries free of charge or at relatively low cost (Lu, 2006). Remote sensing uses both multispectral and hyperspectral sensors, with the former being the most widely used sensor. Examples of multispectral imagers include Sentinel, SPOT 6/ 7 (Satellite Pour I' Observation de la Terre), ASTER (Advanced Spaceborne Thermal Emission Reflection Radiometer) and Landsat 8. The use of these sensors for mapping natural vegetation has become more common because of their suitability for large scale data acquisition without limitation of geographical barriers, which is often the case in the traditional field survey method. Therefore, high-resolution multispectral imageries such as SPOT 6 was used to determine the greenness index of the city of Johannesburg to determine its environmental suitability for its inhabitants.

Odindi *et al*. (2014) used WorldView-2 and SPOT 5 imageries to map bracken fern (*Pteridium aquilinum*) in a conserved urban landscape and found overall accuracy levels of 84.7 % and 72.2 % respectively. In Brazilian Amazon, research using Landsat TM for

biomass estimation was conducted by Lu (2005). Landsat 8-OLI and ETM + data sets have been used to assess above ground biomass of *Eucalyptus* spp and *Pinus* spp in an urban forest plantation (Dube and Mutanga, 2015). They observed that Landsat 8 OLI produced high accuracies for above ground biomass estimation on *P. taeda* (R^2 = 0.69); *E. dunii* (R^2 = 0.71); and *E. grandis* (R^2 = 0.67). A study by Hlatshwayo *et al*. (2019), found high accuracy level (R^2 = 0.70) after deriving AGB of trees in a reforested landfill in Durban, South Africa using SPOT 6 pan-sharpened image. Therefore, SPOT 6 pan-sharpened satellite image with a spatial resolution of 1.5 m was used in this study to map and model plant cover for two urban environments (Soweto and Rosebank suburbs).

1.2. Rationale

Urban greenness is an important indicator of the amount of green space within an urban environment and it contributes to air quality and other ecosystems services (Cilliers and Cilliers, 2016). Vegetation index (VI) refers to a ratio between two or more spectral bands of the electromagnetic spectrum (Xue and Su, 2017). Vegetation index (VI) can be a value that indicates plant vigour of each pixel in a remote sensing image (Fung and Siu, 2000). Urban greenness index refers to a percentage of green space in an urban setting. Urban greenness provides ecosystem services to city dwellers that are crucial to their health quality (Cilliers and Cilliers, 2016). Ecosystems services refer to all benefits (products and services) that humans obtain from ecosystems (Le Maitre *et al*., 2007; Mexia *et al*., 2018), and these are grouped into regulating, provisioning, supporting and cultural services. Ecosystems services provided by urban greenness include carbon sequestration, climate regulation, recreation, habitat for biodiversity, air pollution control (trapping of air pollutants), cooling and noise reduction (Mexia *et al*., 2018; Ngo and Lum, 2018). Nevertheless, urban trees and or green structures are not always about ecosystem services but do also have some disservices. Cilliers and Cilliers (2016) defined ecosystem disservices as the negative impacts of ecosystems on humans or infrastructure. Examples of ecosystem disservices include tree falling, infrastructure destruction, allelopathic substances from poisonous plants and emission of volatile organic compounds (VOCs) (Cilliers and Cilliers, 2016). Therefore, knowledge of ecosystem services and disservices of urban vegetation or greenness is important for urban planning and management.

Urban vegetation in the Johannesburg city is unequally distributed as more vegetation cover is found in rich northern suburbs like Sandton and Rosebank than in poor suburbs like

Alexandra and Soweto (Schäffler and Swilling, 2013). There is more vegetation cover in Northern suburbs (24.2 %) as compared to 6.7 % vegetation cover in Southern suburbs (Schäffler and Swilling, 2013). The rich European settlers of the city planted most of these trees in the affluent suburbs of the cities and thus, they are predominantly alien trees. Because of the previous apartheid regime, many of the informal settlements were designated to host the poor African people with no proper urban setting plans or policies and to date, this gap between the rich and the poor suburbs continue to reflect even after 25 years of democracy. Therefore, the need to quantify plant biomass and carbon, land surface temperature and solar thermal radiation index has necessitated the need to conduct this study which evaluate the present conditions as well as coming up with mitigatory measures to balance the ecological disparity between Rosebank and Soweto areas. Furthermore, this study will provide information gap on the implications of exposure to solar thermal radiation on urban dwellers and benefits of urban greenness.

1.3. Research questions

a) Can the combination of allometric equations and SPOT 6 satellite imageries determine the plant biomass of the suburbs of Rosebank and Soweto in the City of Johannesburg?
b) What is the vegetation index of Soweto compared to Rosebank?
c) What is an environmentally friendly greenness index of Soweto and Rosebank suburbs?
d) What is the land surface temperature of Soweto compared to Rosebank suburb?

1.4. Problem statement

The state of urban vegetation in the city of Johannesburg has not been well quantified. It is, however, crucial to evaluate plant biomass in relation to an urban population to improve urban green infrastructure to address such changes. Several studies on above ground biomass (AGB) of trees in forest stands have been documented (Nelson *et al*., 1999; Ketterings *et al*., 2001; Lu, 2006; Gibbs *et al*., 2007; Avitabile *et al*., 2012; Dube and Mutanga, 2015). Estimation of the AGB is important because it is related to air quality, the health status of city dwellers and carbon storage potential of trees in an ecosystem. In addition, urban trees play a crucial role in the global carbon cycle by trapping and storing atmospheric carbon dioxide through the process of carbon sequestration. Street trees and urban forest are largely concentrated in wealthier suburbs, but not in the informal settlements because most of the trees in Johannesburg are the legacy of the European arrivals to South Africa. Thus, marginalized suburbs such as Soweto, a township south of Johannesburg, do not have the

privilege of ecosystem services provided by street trees and other green spaces. Soweto is experiencing population increase and this has resulted in rapid infrastructure development to address rising demand for housing. The increase in urban population threatens the urban environment through storm flooding and increased urban heat island. Infrastructure development like construction of buildings , tarred and concrete structures contribute to a rise in land surface temperature. Nevertheless, the actual urban street trees and other green vegetation in the city have not been well established, and therefore this study investigated this gap of greenness in two suburbs of the city of Johannesburg (Soweto and Rosebank). The role of urban greenness on land surface temperature characteristics of the two areas has not been evaluated thus, Landsat 8 satellite data was be used to analyse the urban heat island effect.

However, with recent advancement in new high-resolution satellite imageries like WorldView-2 and SPOT6/ 7, their application in vegetation mapping and biomass estimation has increased. This study, therefore, quantified and modelled plant biomass of the two suburbs based on SPOT 6/7 satellite image and the findings are expected to contribute to urban greening policy planning in future, and more particularly to facilitate tree planting in the biggest township of Johannesburg, Soweto. It will develop an environmentally friendly greenness index based on a ratio between the total area of a city or suburb covered by green vs. the total area of a city or suburb. This index will guide urban greening policy planning in future as the world is moving towards more environmentally friendly cities.

1.5. Aim and objectives

The main aim of this study was to investigate the greenness index of the city of Johannesburg to determine its environmental suitability for its inhabitants.

The main objectives of this study were:

a) To measure plant biomass using allometric equations and SPOT 6 satellite imageries in the two urban environments of Johannesburg (Soweto and Rosebank).
b) To determine the vegetation index of Soweto and Rosebank for urban environment condition analysis using SPOT 6 data.
c) To compute an environmentally friendly greenness index based on a ratio between the total area of a city or suburb covered by green vs. the total area of a city.

d) To determine the urban heat island using thermal Landsat 8 data in Rosebank and Soweto as case study areas.

CHAPTER 2: LITERATURE REVIEW

2.1. History of urban greenness in the city of Johannesburg

History of trees in the city of Johannesburg dates to the period of gold discovery in the 1880s when the European colonialists planted gum trees which were used as props in the mines (Buff, 2012). In addition, trees like *Eucalyptus* were planted for the purposes of trapping the dust from mine dumps (Turton *et al*., 2006). The first trees to be planted in the Johannesburg city were the oak, jacarandas, walnut and gum trees (Buff, 2012); however, indigenous trees of *Combretum erythrophylum* and *Acacia sieberiana*-subspecies woodii were also planted. Most of these trees were introduced for fuel, fruit, fodder and wood production (City of Johannesburg, 2013). It is recorded in history that William Nelson by 1896 had grown 30 million jacaranda trees, shrubs and plants in his Nelsonia Nurseries for free distribution of this species (Buff, 2012).

Presently, there are more than 10 million estimated trees in Johannesburg city (Schäffler and Swilling, 2013). The trees are mostly found inside private people's gardens, parks, cemeteries, conservation areas, streets and on city pavements. Urban trees in the city of Johannesburg are not well distributed because the European settlers split Johannesburg into north rich suburbs with dense green vegetation and poor south suburbs such as the township of Soweto with a low number of green trees and or vegetation (Buff, 2012). However, to address this ecological disparity, the government launched the Greening Soweto project in 2006, aiming to beautify Soweto by planting trees (City of Johannesburg, 2013). The Johannesburg City Park was responsible for project implementation, management and conservation of trees in the city of Johannesburg. The project targeted the planting of 200 000 trees for five years in Soweto to improve its urban greenness. (City of Johannesburg, 2013). The Greening Soweto project became part of five years (2006-2011) of the Integrated Development Plan.

2.2. Importance of urban greenness

Urban greenness represents an important fundamental aspect of any urban ecosystems. Urban trees play a significant role in minimizing carbon dioxide (CO_2) through carbon sequestration and carbon emission reduction from power plants, vehicles and urban traffic (Myeong *et al*., 2006). This helps minimize climate change at global scale whilst at a local and regional scale it contributes to better air quality. According to Shekhar and Kumar (2014), urban greenness

plays a major role in urban centres through the provision of aesthetic, ecological, public health and quality of life. Ecological benefits of urban greenness include carbon sequestration, provision of shelter, feed and water for biodiversity. Trees exhale out oxygen, and inhale in carbon dioxide during the photosynthetic process, and filter harmful air pollutants, which helps maintain the ecological balance of urban ecosystems.

According to a study by Nowak *et al*. (2007) on the effects of urban forest and value in San Francisco city, USA. *Eucalyptus globulus* trees could sequester 847 tons of carbon per year. However, when these trees die the same quantity of stored carbon is released again into the atmosphere (Nowak *et al*., 2007). Annual carbon sequestration is related to the health status of trees and depends on the diameter of the trees (Nowak *et al*., 2007). Thus, healthier trees with larger diameters sequester more carbon per year. Importance of urban vegetation includes biodiversity preservation, reducing urban heat island, cooling of the atmosphere, reducing flooding and soil erosion (WHO, 2016). The various services and benefits offered by urban greenness depend on management activity, therefore a decline in tree health could lead to a decrease in services and benefits. The information of urban greenness is helpful to urban planners for attaining environmental management goals, thus contributing to the achievement of sustainable development goals (Shekhar and Kumar, 2014).

2.3. Plant biomass estimation using nondestructive methods

Plant biomass encompasses the above and the belowground living forms including all plants and dead materials of litter attributed to the soil (Lu, 2006). Plant biomass shows the amount of carbon that can be emitted (carbon dioxide) when vegetation is cleared or burned (Vashum and Jayakumur, 2012). Most researches focus on the estimation of AGB since it is easy to conduct field data collection. It helps in the estimation of the quantity of CO_2 that is trapped by vegetation from the atmosphere (Vashum and Jayakumur, 2012). Plant biomass can be estimated directly with remote sensing data from various techniques (Kumar and Mutanga, 2017) and estimated indirectly from structural parameters (Nowak, 1993). Destructive sampling is the most widely used indirect method for estimating above-ground plant biomass (Gibbs *et al*., 2007; Vashum and Jayakumur, 2012). Although destructive sampling method gives an accurate measure, it is expensive, resource and time consuming and destructive in nature and therefore not suitable for large area assessment (Ketterings *et al*., 2001; McHale *et al*., 2009; Kumar and Mutanga, 2017; Ngo and Lum, 2018). Since this method requires cutting down of trees, it is not practical to weigh all biomass for each tree in an urban area

(McHale *et al*., 2009). For instance, Ngo and Lum (2018) successfully estimated urban tree AGB of tropical street trees using a destructive method. Nevertheless, they observed that equations for tropical trees overestimated AGB of street trees. On the other hand, a nondestructive method does not involve tree felling, although the method has limitation since it is difficult to validate its reliability for biomass estimation (Vashum and Jayakumur, 2012). Nevertheless, the nondestructive method is still better and environmentally friendly for large scale biomass estimation of urban vegetation compared to the destructive method. Therefore, estimation of AGB of urban trees is vital for policy formulation and tree planting initiatives which ultimately contributes to the planning of greener and friendly cities.

2.4. Estimating plant biomass using remote sensing

Remote sensing involves a technique of obtaining information about an object without being in contact with the object (Bhandari *et al*., 2012; Vashum and Jayakumur, 2012). It uses either satellite or aircraft-based technologies to detect and classify objects on earth. Three ways of capturing information through remote sensing include aeroplane, satellite and drone. Estimating the AGB with remote sensing method gives a reasonable and less expensive means of obtaining data on a larger scale (Xie *et al*., 2008; Xie *et al*., 2009; Sousa *et al*., 2015). Remote sensing can cover large areas and has high temporal frequency and is cheaper compared to ground-based assessment (Lu, 2006; Kumar and Mutanga, 2017). The high-resolution satellite imageries allow mapping the above ground biomass at local and national scales with high levels of accuracy (Lu, 2006). Although remote sensing is useful for biomass estimation, it does not give the exact amount of biomass available in an area (Vashum and Jayakumur, 2012). It measures tree structural parameters, which are correlated to biomass (Vashum and Jayakumur, 2012). Selection of remote sensing imageries is affected by three factors: mapping cost of images, climatic conditions (for example temperature) and technical issues for image interpretation (Vashum and Jayakumur, 2012). Therefore, plant biomass can be derived through remote sensing and field measurements from which allometric equations are developed.

Multispectral remote sensing refers to collection or measurement of reflected energy from 3 to more than 10 bands of the electromagnetic spectrum and hyperspectral remote sensing involves the collection of energy in narrower bands of more than 200 bands in the electromagnetic spectrum (Zhang *et al*., 2018). Examples of hyperspectral imagers include Airborne Visible/ Infrared Imaging Spectrometer (224 bands) and Hyperion Imaging

Spectrometer (220 bands) with 0.4 - 2.5 µm wavelength. Hyperspectral sensors enable surface features detection, identification and quantification through pixel analysis of an image (Zhang *et al*., 2018). Also, it allows the mapping distribution of materials and can easily detect material or object uniqueness in a scene (Govender *et al*., 2008). Hyperspectral remote sensing allows mapping of dense urban vegetation with high accuracy level due to the larger number of spectral bands. Liu *et al*. (2017) successfully mapped 15 urban tree species in Surrey City, Canada using hyperspectral and LiDdar remote sensing and their overall accuracy levels for individual tree species was between 51 and 70 %.

In the past multispectral sensors were only able to map trees at genus level thus identifying individual tree species within each genus was not possible (Govender *et al*., 2008). However, the new satellite sensors like Worldview 2 and Sentinel 2 with 8 and 13 spectral bands, respectively can now discriminate between species (Immitzer *et al*., 2012). However, there is an increased level of complexity and redundancy with Hyperion Imaging Spectrometer data due to a bigger number of spectral bands. Multispectral imageries take images in multiple wavelengths of the electromagnetic spectrum and the spatial resolution (low, medium and high) varies with the wavelength. Examples are SPOT 6/ 7, Landsat 8 and ASTER (Abrams, 2000; Lu, 2006). Remote sensors are sensitive to vegetation characteristics like shadow, texture and tree density (Sousa *et al*., 2017). Sousa *et al*. (2017) noted that with passive sensors it is difficult to classify and differentiate tree canopies due to large pixel size. High spatial resolution imageries such as QuickBird and IKONOS are more expensive than medium spatial resolution imageries (Landsat 8 and ASTER) (Lu, 2006). High spatial resolution images for plant biomass estimation are costly and require more time for image processing (Lu, 2006). Therefore, high multispectral resolution imagery like SPOT 6 was used in this study.

2.5. Vegetation indices

Vegetation index (VI) represents a ratio of two or more spectral bands (Xue and Su, 2017). VIs helps in demarcating distribution of vegetation and soil characteristic reflectance of green vegetation (Bhandari *et al*., 2012). It can be correlated with field measured variables such as biomass (Xue and Su, 2017) and this is significant in highlighting patterns of green vegetation distribution (Fung and Siu, 2000). Atmospheric and topographic effects, soil background and changes in sun and viewing angles affect reflectance from vegetation in different wavelength bands (Bhandari *et al*., 2012). Several VIs can be applied in biomass

estimation but the most widely used is the Normalized Difference Vegetation Index (NDVI) (Fung and Siu, 2000; Mutanga and Skidmore, 2004b). In this study, NDVI was selected because it is highly beneficial for policy planners since it can easily provide a clear distinction of surface features like green and non-green areas (Gandhi *et al*., 2015). In addition, this promotes easy prediction of areas affected by disasters, or anthropogenic activities and those that require protection or maintenance strategies (Gandhi *et al*., 2015). The NDVI can also provide a linkage of the city socioeconomic way of life for example rich people are associated with areas with high vegetation densities and less populated areas. In a study by Fung and Siu (2000), NDVI obtained from the multispectral SPOT imagery was used to assess the environmental quality of Hong Kong city over a four-year period. They observed that NDVI values were highly associated with high-density urban areas and level of crowdedness. Also, an increase in NDVI values was noted in areas subjected to landscape improvement and low NDVI values in areas undergoing urban expansion (Fung and Siu, 2000). However, NDVI focus on changes in productivity disregarding land use changes in an area. From the above-mentioned strengths that's why NDVI was selected as vegetation index to evaluate the urban environmental quality life of city dwellers in Rosebank and Soweto areas.

Some other methods of calculating vegetation indices for urban environment analysis condition include Enhanced Vegetation Index (EVI), Transformed Vegetation Index (TVI), Simple Ratio (SR) and Modified Normalized Difference Vegetation Index (MNDVI) (Xie *et al*., 2009). Mapping vegetation changes, land cover and land use changes are done with remotely sensed data. Plant biomass estimation using remote sensing techniques is mainly based on NDVI datasets. Lu (2006) noted that not all vegetation indices are directly related to above-ground biomass. Therefore, NDVI was calculated to determine the health status of vegetation cover and environmental quality in Rosebank and Soweto suburbs in the city of Johannesburg.

2.6. Urban heat island

Studies of urban heat islands are well documented in the literature (Sun *et al*., 2012; Shekhar and Kumar, 2014; Abutaleb *et al*., 2015; Hardy and Nel, 2015; Xue and Su, 2017; Xue *et al*., 2017; Kaplan *et al*., 2018; Orimoloye *et al*., 2018). The urban heat island (UHI) analysis through estimation of land surface temperature (LST) can provide valuable information on the health status of people living in urban areas (Orimoloye *et al*., 2018). Land surface

temperature estimation provides a better understanding of UHI analysis and as an input for model development. There has been an upsurge in the application of remote sensing techniques like Landsat 5 TM (Buyadi *et al*., 2014), Landsat 7 ETM+ (Abutaleb *et al*., 2015; Pal and Ziaul, 2017) and Landsat 8 (Ogunode and Akombelwa, 2017; Xue and Su, 2017; Kaplan *et al*., 2018; Orimoloye *et al*., 2018) imageries for deriving land surface temperature (LST) to evaluate effects of urban heat island. The UHI is defined as urban areas or cities that are warmer than surrounding areas because of human activities (Hardy and Nel, 2015; Kaplan *et al*., 2018). Also, according to Abutaleb *et al*. (2015), urban heat islands refer to areas where temperatures are higher close to urban centres and lower temperatures near the urban periphery. Land surface temperature and vegetation indices indicate the impacts of built-up areas and green areas on UHI (Kaplan *et al*., 2018). Hardy and Nel (2015) asserted that the density of people, low vegetation cover and buildings in highly populated urban areas exacerbate the effects of urban heat island.

Green or vegetated areas have a profound effect on urban heat island by providing shade and evapotranspiration (dos Santos *et al*., 2018). Similarly, land cover change and rapid urbanization can accelerate LST and solar thermal radiation (Orimoloye *et al*., 2018). Abutaleb *et al*. (2015) observed a similar pattern of increased land surface temperature in high population density areas in Greater Cairo as a result of urban areas expansion. In addition, a study conducted in Skopje, Macedonia showed a negative correlation between LST and NDVI (Kaplan *et al*., 2018). Some of the factors that play an important role in the formation of UHI, for example, black impermeable surface like concrete surfaces which absorbs heat and remove moisture from the air which ultimately affects the air-cooling characteristics (Alhawiti and Mitsova, 2016). Planting of more street trees and creating new parks helps to address the impacts of urban heat island for urban dwellers (dos Santos *et al*., 2018). Therefore, deriving LST from Landsat 8 data is important for the assessment of UHI of Rosebank and Soweto suburbs.

CHAPTER 3: METHODOLOGY

3.1. Description of the study areas

Soweto is a suburb in the city of Johannesburg, Gauteng province, (South Africa), located at latitude 26°15′58″S and longitude 27°51′57″E and covers an area of 224.80 km^2. Soweto was founded in 1963 when white dominated 'the apartheid regime' decided to separate Blacks from Whites. Soweto is an abbreviation for South Western Townships, and it lies at 1632 m above sea level. The Soweto suburb is dominated by Black Africans constituting 98.5 % of its total population and the rest is made up of Coloured, Indian/Asian, Whites and others (http://www.statssa.gov.za/2011 Census). Soweto is 20 km south of Johannesburg city (Figure 3.1). Its climate is warm, temperate with high rainfall in summer, and low in winter. The average annual temperature is 15.8 °C and rainfall is 750 mm. The common trees in Soweto include *Rhus lancea*, *Celtis africana*, *Eucalyptus* species and *Combretum erythrophylum*.

Rosebank is a suburb found in Randburg on the Northern parts of Central Johannesburg and is located at latitude 26°8′43″S and longitude 28°2′26″E and occupies an area of 30.4 km^2 with. It is 12.2 km from the center of Johannesburg city (Figure 3.1). Black Africans constitute 48.7 % of the population and the rest is composed of Indian/ Asian, White, Coloured and others (http://www.statssa.gov.za/2011 Census). It lies at an elevation of 1660 m above sea level. Some of the common trees found in this suburb include jacaranda (*Jacaranda mimosifolia)*, London plane (*Platanus acerifolia*), *Eucalyptus* species and Oak tree (*Quercus* species).

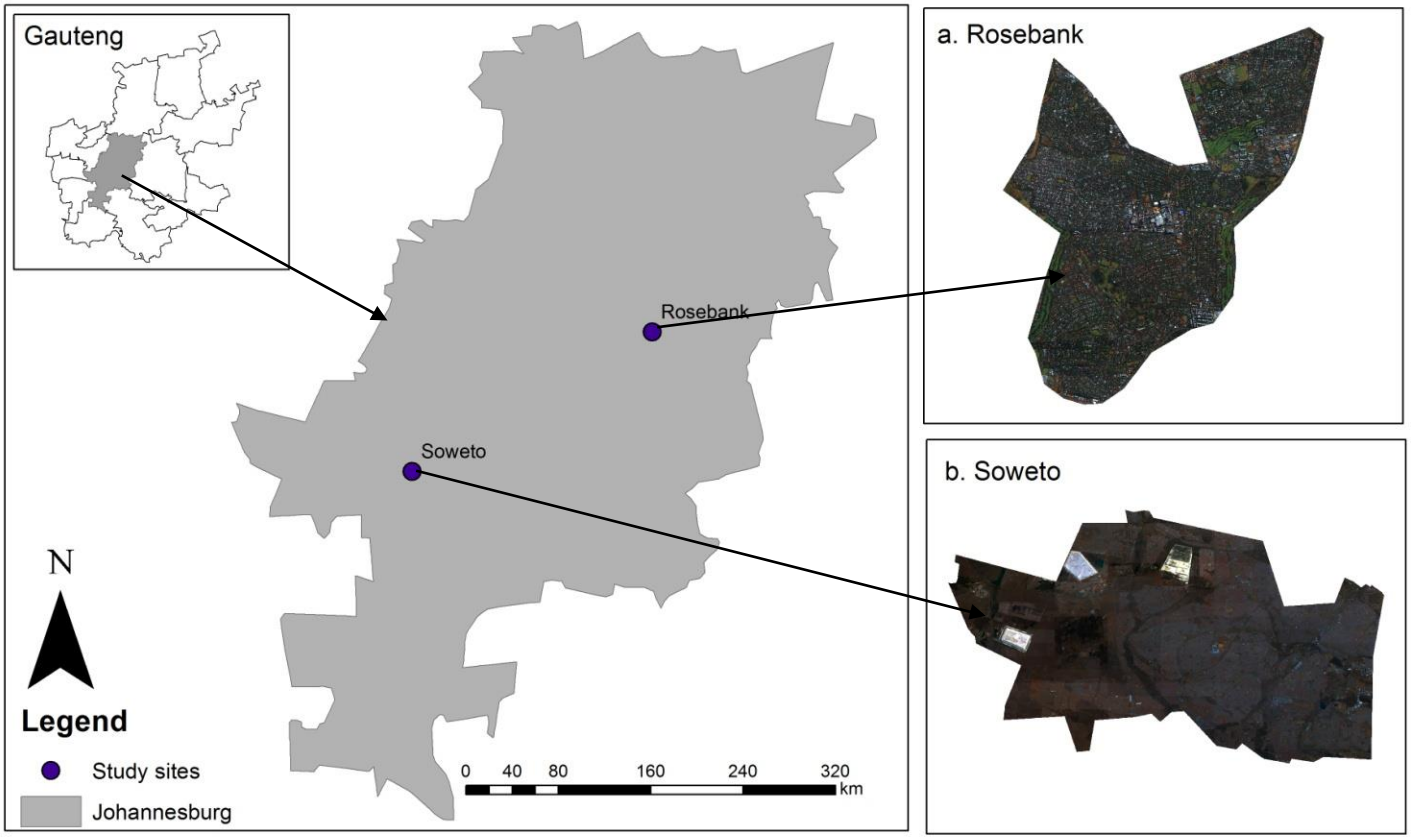


Figure 3.1: Location of study areas of Rosebank and Soweto suburbs in Johannesburg.

3.2. Experimental design

A random sampling procedure was used in this study based on the streets. A random starting point was selected using a street map of Rosebank. Fieldwork was carried to obtain in-situ data of circumference at breast height (CBH) and tree location. Stem or trunk circumference was measured for all trees at every 50-100 m apart in each selected street of Rosebank suburb. Tree location was recorded using Garmin Etrex 10 (South Africa) handheld receiver global positioning system (GPS) and tree stem circumference were measured using a tape measure. The trees diameters of was estimated from stem/trunk circumference (CBH). Therefore, DBH and radius were derived from equation (1) and equation (2) respectively as follows;

$$\mathrm{DBH} = \frac{\mathrm{CBH}}{\pi} \quad \text{……(1)}$$

$$\mathrm{r} = \frac{\mathrm{DBH}}{2} \quad \text{……(2)}$$

Where DBH is diameter measured at 1.3 m, CBH is stem circumference at 1.3 m, π = 3.142 and r is the stem radius.

3.3. Biomass estimation

Two methods of estimating above ground biomass used in this study are species-specific allometric equations and remote sensing data.

3.3.1. Field biomass estimation using the allometric equations

Most allometric equations for biomass estimation aim to establish a relationship between physical parameters (tree height and diameter) and above ground biomass estimated using non-destructive method (Ketterings *et al*., 2001; Vashum and Jayakumar, 2012). There are two types of the allometric equation which include general and species-specific. When selecting a method for plant biomass estimation, the applicability of that method for an area or tree species must be considered. In this study, species-specific allometric equations by McHale *et al*. (2009) were used to estimate biomass considering the DBH of the trees as an important input.

In the absence of a species-specific equation, a general equation may be used to derive the above ground biomass of trees (Tietema, 1993). The use of general allometric equations may solve the problem of high variability and uncertainty related to the use of species-specific allometric equation for urban environments (McHale *et al*., 2009). Kim *et al*. (2011) asserted

that site-specific allometric equations give an accurate prediction of plant biomass at a local scale since it considers site effects (such as soil fertility). Most of the trees in the study areas occur along streets, which makes it difficult for any estimation of biomass using the destructive method. In this study, 120 trees were measured for stem circumference to calculate biomass. Biomass estimation using allometric equation methods was therefore used in this research as indicated in equation (3) and (4):

$$Jacaranda\ mimosifolia = 0.028317(0.036147) * (\frac{dbh}{2.54})^{2.48628} * 609 \text{.....(3)}$$

$$(Platanus\ acerifolia) = 0.028317(0.025170) * (\frac{dbh}{2.54})^{2.673578} * 833 \text{..... (4)}$$

Where dbh is diameter at breast height measured at 1.3 m above ground level.

Estimation of Carbon content in AGB

After obtaining the AGB of *Jacaranda mimosifolia* and *Platanus acerifolia* for Rosebank suburb, the amount of carbon stored was determined based on equation (5). Also, the total Carbon in Rosebank and Soweto was estimated from the total above ground biomass (AGB) obtained from SPOT 6 pan-sharpened image. According to Martin and Thomas (2011), the carbon content of trees in above ground biomass ranges from 45 to 55 %. Therefore, in this research, an equation by Martin and Thomas (2011) was considered and it assumes that carbon content is obtained by multiplying total AGB by 45 % (biomass conversion factor). The conversion factor is not always 0.45, for example in a study by Chave *et al*. (2005) the carbon content in AGB calculated using 0.5 as their conversion factor.

$$\Delta AGB = AGB * 0.45 \text{.....(5)}$$

Where ΔAGB is Carbon quantity in above ground biomass and AGB is above ground biomass.

3.3.2. Extraction of AGB from SPOT 6 satellite images

The Normalized difference vegetation index (NDVI) pixel values were obtained from SPOT 6 pan sharpened image. Pearson correlation was performed to determine the relationship between estimated AGB-(dependent variable) of trees recorded in Rosebank suburb and SPOT 6 pan-sharpened image band values (independent variables). This was done to determine bands that are best predictors of above ground biomass. SPOT 6 band values were extracted through overlaying 120 ground points on the Rosebank NDVI layer and this was performed in Arc GIS 10.5 software. As highlighted by Hlatshwayo *et al*. (2019) and Muhd-

Ekhzarizal *et al*. (2018) a model with the highest r^2 value should be considered the best estimator of AGB. Therefore, predictor variables that had the highest r^2 values were considered for modelling in this study. The following steps were considered for deriving AGB from SPOT 6 satellite image:

- Estimation of Above ground biomass of each tree recorded in Rosebank suburb during field work using two species-specific equations for *Platanus acerifolia* and *Jacaranda mimosifolia* trees.
- Calculation of NDVI of the image, extraction of NDVI values based on 120 ground points and four band values using Arc tools in Arc Map 10.5.
- Creating a scatter plot of linear function graphs of AGB vs. band values and AGB vs. NDVI values.
- Developing a model of the image that estimates AGB based on the best predictor variables.

It was necessary to perform resampling of the SPOT 6 image into a window size of 4 x 4 since biomass estimated per each tree was not equivalent to one pixel. This method involves combining several pixels through aggregation and obtaining the mean pixel value. The maps of total AGB and carbon content for Rosebank and Soweto areas were produced in R3.4.1 software.

3.4. Field data collection

Ground truthing data collection in Rosebank suburbs of Johannesburg city was conducted in July 2018. A total of 120 GPS points was collected from street trees (62 *Platanus acerifolia* and 58 *Jacaranda mimosifolia*) in Rosebank. However, no ground truthing data was recorded from Soweto suburb due to unavailability of big trees and more specifically the two common species found in Rosebank along the streets. Big trees that were found in Soweto suburb occurred at former mining sites and the research was not focusing on mining areas, therefore they were disregarded. Some big trees encountered in Soweto fall in the yards of residences which the researcher had no access to measure DBH. Similarly, trees found along streets in Soweto were *Acacia trifoliata*, *Rhus lancea* and *Celtis Africana* which were planted by the City Parks during the Greening Soweto programme of 2006. Field data collected in Rosebank suburb was used to derive AGB and through digitizing 13 polygons per each class (white built-up, brown built up, other vegetation, water, swimming pool, grasses and bare soil) for random forest classification and overlaying in Arc Map 10.5. Since there were no

ground truthing points for Soweto, a model was developed for Rosebank and fitted into Soweto study area.

3.5. Remote Sensing Data

In this study, SPOT 6 and Landsat 8 were used as remote sensing data sets, and these were obtained from SANSA and USGS website respectively. Both sets of satellite images were acquired in winter 2018.

3.6. Image acquisition and processing

SPOT 6 winter imageries covering Soweto and Rosebank suburbs in the City of Johannesburg (CoJ) were obtained free of charge from South African National Space Agency (SANSA) on 9 June 2018 closer to July 2018 to match the date of the field data collection. SPOT 6 was used because it was available free of charge from SANSA as compared to other satellites that require purchase of the images. In addition, SPOT 6 satellite's capability of a daily revisit to a scene increases the probability of capturing images with a high level of accuracy (Sousa *et al*., 2015). Winter images were used in this study since most of the trees and grass species were still green and this reduced bias compared to images that would have been taken in August during the windy periods. Also, summer images would be difficult to detect the greenness since most trees would shed their leaves and some might have grey leaves. The two satellite images were already orthorectified and registered to Universal Transverse Mercator (zone 35 South), hence there was no need to perform image preprocessing steps. The panchromatic spectral resolution of SPOT 6 is 1.5 m while its multispectral resolution is 6 m and image swath of 60 km (Sousa *et al*., 2015). SPOT 6 has a spatial resolution of 1m TerraSAR-X and TanDEM-X radar satellite and better resolution with 15 km ortho image products (Sousa *et al*., 2015). The spectral bands of SPOT 6 include; green (530-590 µm), blue (450- 525 µm), red (625- 695 µm), panchromatic (450- 745 µm) and near-infrared (760-890 µm) (Sousa *et al*., 2015). Remote sensors are sensitive to vegetation characteristics like shadow, texture and tree density (Sousa *et al*., 2015).

3.7. Image classification

The SPOT 6 imageries of Rosebank and Soweto were classified using the random forest (RF) algorithm. A pixel-based classification was selected because it has an advantage of classifying images more quickly as compared to other classification methods like object-based (Shojanoori *et al*., 2016). With pixel-based classification, it is easy to perform analysis

of the spectral properties of all the pixels in a region of interest. The two study areas were classified into seven classes namely *Jacaranda mimosifolia*, *Platanus acerifolia*, other vegetation, grasses, built up (white and brown), bare soil, water and swimming pool (Table 3.1). Image processing was performed using Arc Map 10.5 and ENVI 5.3 software. Image classification was performed to classify every pixel in an image into different classes (Shalaby and Tateishi, 2007). Random forest classification was performed in R3.4.1 software (R Core Team, 2016).

Table 3.1: Land cover classes of Rosebank and Soweto suburbs in Johannesburg selected for Random Forest classification.

Land cover class	Description
Built-up (white and brown)	all commercial and residential areas as wells as roads and concrete/ paved surfaces
Jacaranda	all jacaranda trees species
London plane	all London plane tree species
Other vegetation	other woody vegetation, not jacaranda or London plane trees
Bare soils	all areas with exposed soil
Grasses	all areas covered by grasses
Water	all natural and man-made water bodies including zoo lakes, rivers and dams
Swimming pools	all pools inside people's homes and those in public recreational places

3.7.1. Random Forest classification

The Random forest is a classification algorithm and learning technique in which each tree contributes a single vote for assignment of the most frequent class to the input (Breiman, 2001; Gislason *et al*., 2006). Since each tree vote for the popular class, the classification output is determined by majority vote of the trees (Gislason *et al*., 2006). Random Forest (RF) requires ntree-number of trees and mtry- maximum number of features for optimization (Adam *et al*., 2012). The Random Forest draws sets of new training samples from the original set of the training set and the drawn set is replaced (Breiman, 2001). With the use of random feature selection, a tree is grown on the new selected training set (Breiman, 2001).

The random forest then selects a class with the highest number of the vote out of total votes (N votes) for that case (Pal, 2005).

The random forest classifier has the advantage of completing the selection of features through automatic grouping the importance of variables (Adam *et al*., 2012). Also, another strength of the RF classifier is that grown trees are not pruned (Breiman, 2001). The number of variables and trees are the two parameters that can be adjusted in the random forest and they can vary based on user decision, hence it is a user-defined parameter (Pal, 2005; Gislason *et al*., 2006). Random Forest (RF) classification algorithm can easily produce accuracy and variable importance tables. In addition, the RF algorithm can handle both continuous data sets or discrete data and easily deal with large quantities of data sets (Gislason *et al*., 2006). Figure 3.2 shows the steps that were taken for SPOT 6 image analysis.

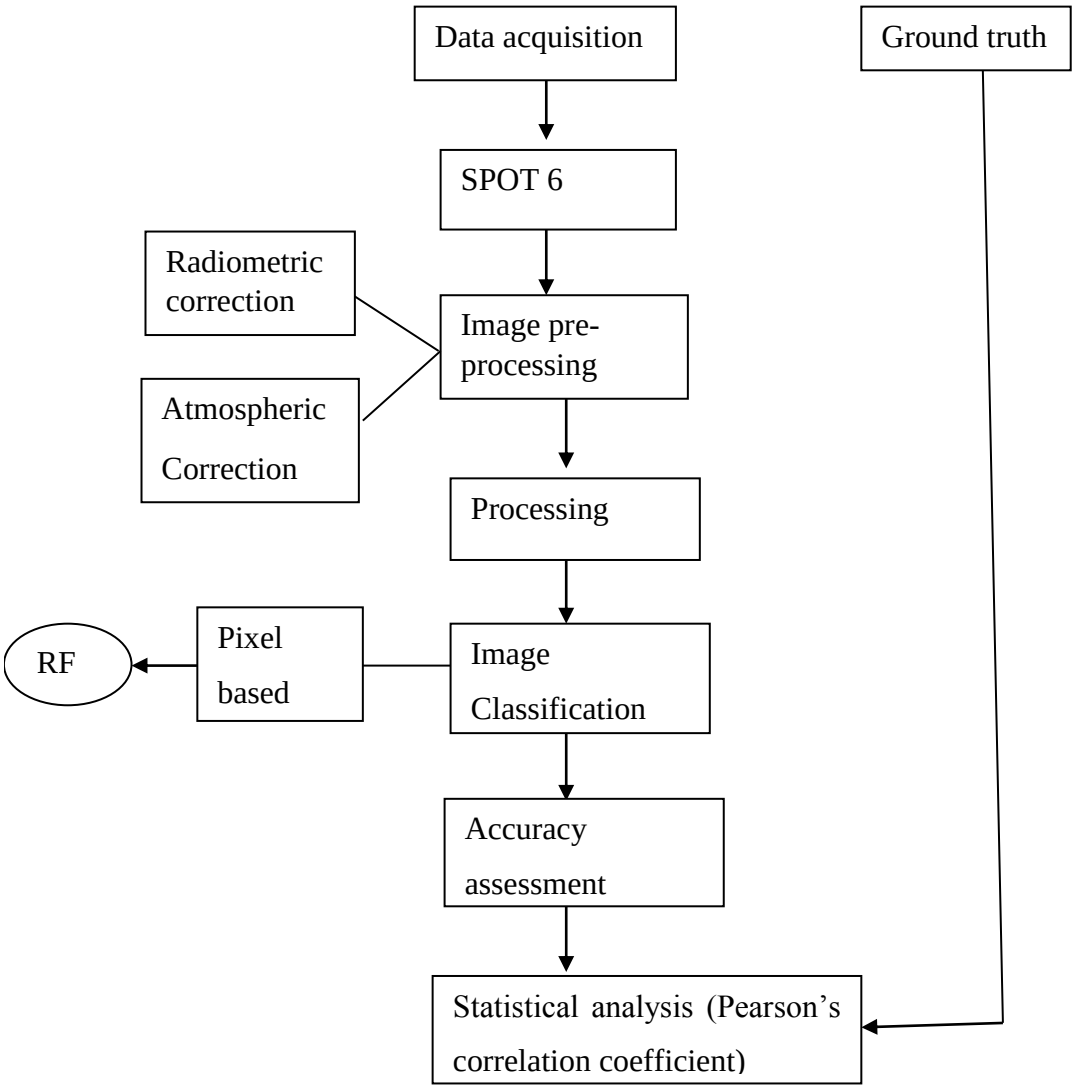


Figure 3.2: Flow chart diagram showing steps of SPOT 6 image analysis.

Greenness Index

The evaluation of urban greenness is important for planning purposes and it gives information on the environmental quality of cities. Shekar and Kumar (2014) proposed a method of estimating green index based on classifying NDVI values into green and non-green classes. Similarly, Yang *et al*. (2009) suggested a method called green index to assess urban vegetation and it was calculated as the percentage of total area of green of four pictures to the total area of the four images. Therefore, in this study, the green index was modified to derive the greenness index and it was calculated as the percentage of an area of green classes divided by area of each suburb. After performing random forest classification, the area coverage for each land cover category was obtained. In this research, three vegetation classes were considered for calculation of greenness index of Rosebank and Soweto suburbs and these are *Jacaranda mimosifolia*, *Platanus acerifolia* and Other vegetation.

$$\text{Greenness index} = \frac{\text{Area covered by green}}{\text{Total area of study area}} \quad \ldots\ldots(6)$$

3.8. Vegetation index

Normalized difference vegetation index (NDVI) refers to a ratio combination of near-infrared and visible red bands (Rouse *et al*., 1974). It is centred on the observation that chlorophyll in green leaves absorbs light in the NIR region. The NDVI shows greenness occupying a pixel. NDVI may be used as an indicator of the greenness of the vegetation (Bhandari *et al*., 2012) and correlates with vegetation's photosynthetic activity (Wang and Tenhunen, 2004). Its values range between -1 to +1; large positive NDVI values show dense vegetation and water has negative NDVI values (McFeeters, 1996; Kaplan *et al*., 2018). According to Bhandari *et al*. (2012), NDVI values of 0.1 and below represent barren of rocks, snow or sand, moderate values (0.2 to 0.3) represent shrub and grassland and high values represent tropical and temperate areas. Similarly, in a study by Shekhar and Kumar (2014) all negative NDVI values were considered as non-green and positives as green. NDVI values were re-classified into four classes following a method adapted from Shekhar and Kumar (2014) (Table 3.2) and this was performed using Arc GIS 10.5 under reclassify option in Arc Tools. Therefore, the NDVI values of the two SPOT 6 satellite images were calculated using the following equation (Rouse *et al*., 1974).

$$NDVIi = \frac{NIRi - Redi}{NIRi + Redi} \quad \ldots\ldots(7)$$

Where NDVI is the normalized difference vegetation index; NIR is near infrared band; Red is Red band; *i* is the pixel position in the scene (R = 3 and NIR = 4).

Table 3.2: Description of Normalized difference vegetation index (NDVI) classes for Rosebank and Soweto suburbs.

Normalized difference vegetation index class	Description
-0.999- 0.25	Low green quality
0.25- 0.5	Moderate green quality
0.5- 0.75	High green quality
0.75- 0.999	Very high green quality

3.9. Urban heat island

The Thermal Infrared Sensor (TIRS) of Landsat 8 satellite imagery was used to obtain land surface temperature (LST) of Rosebank and Soweto areas based on steps in Figure 3.3. The Landsat 8 imagery covering both Soweto and Rosebank was downloaded free of charge from the United States Geological Survey (USGS) web link (https://glovis.usgs.gov/). The downloaded standard level 1 Landsat 8 image had cloud cover of 0.12 % and was acquired on 22 July 2018 in the morning. The sun's azimuth and elevation were 37.66° and 33.90° respectively. The image was also registered in Universal Transverse Mercator (UTM- 35 North) projection using WGS 84 coordinate system. There are two sensors of Landsat 8 satellite imagery namely Thermal Infrared Sensor (TIRS) and Operational Land Imager (OLI) (Adiri *et al*., 2017). The OLI has 4 bands in Visible (0.43- 0.67 µm), NIR band (0.85- 0.88µm), 2 SWIR bands (1.57- 2.29 µm) and Cirrus (1.36- 1.38 µm); Panchromatic band (0.50- 0.68 µm) with 15 m resolution (Orimoloye *et al*., 2018). The TIRS has two bands TIRS 1 (10.6- 11.19 µm) and TIRS 2 (11.5- 12.51 µm) (Adiri *et al*., 2017). Landsat 8 spatial resolution lies between 15 and 100 m and has a temporal resolution of 16 days (Lu, 2006; Anandababu *et al*., 2018). Thus, satellites with long revisit time have low probability of obtaining cloud-free high-resolution data over areas prone to cloudy conditions (Hardy and Nel, 2015). Landsat 8 is cost-effective in terms of data acquisition, freely available for use and a single scene covers an area of 185 x 180 km (Roy *et al*., 2014; Anandababu *et al*., 2018).

The Land surface temperature was derived from Landsat 8 satellite image (Figure 3.3) for urban heat island analysis and was calculated following equations below (Carlson and Ripley, 1997; Jiménez-Muñoz *et al*., 2014; USGS, 2016). All steps were performed using Arc GIS 10.5 software. Digital numbers (DN) were changed to top of atmosphere (TOA) radiance and brightness temperature was derived from TOA radiance using rescaling factors given in the Landsat 8 metadata file (USGS, 2016). Atmospheric correction of the Landsat 8 image was performed using the FLAASH method in ENVI software version 5.3. and LST maps of Rosebank and Soweto were created using Arc Map 10.5. The input image for atmospheric correction was the radiometrically calibrated radiance image. The major reason for performing atmospheric correction was to get rid of the noise effects from dust and water vapour in the atmosphere on the image. The Landsat 8 image was re-projected to UTM 35 South using WGS-84 coordinate system.

In this study, band 10 of the TIRS was used to estimate brightness temperature (equation 8). Normalized difference vegetation index values of Rosebank and Soweto areas were derived from the corrected Landsat 8 image using bands 4 and 5 and the metadata file (MTL-file) provided in the Landsat 8 imagery. A flow diagram of Landsat 8 data processing is illustrated in Figure 3.3. After retrieving LST from Landsat 8 satellite data, an ecological evaluation index (UTFVI) was calculated to quantitatively investigate the effects of UHI intensity on Rosebank and Soweto suburbs. Furthermore, Global Solar ultraviolet (UV) index was also derived from LST to evaluate the effects of prolonged solar ultraviolet radiation exposure on the health of people living in the two suburbs of Johannesburg.

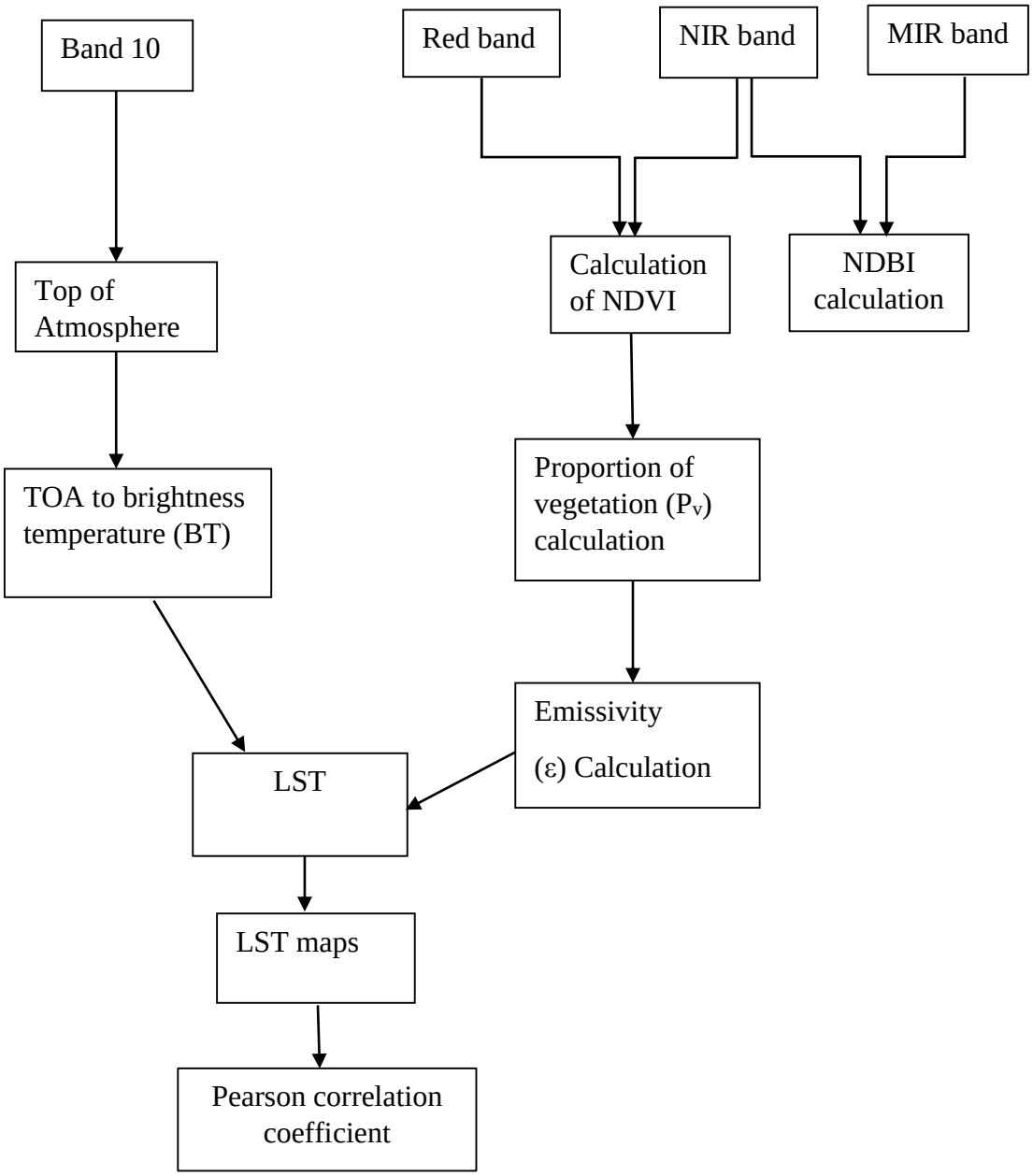


Figure 3.3: Flow chart diagram for land surface temperature (LST) calculation using Landsat 8 data.

3.9.1. Top of Atmospheric (TOA) spectral radiance calculation

There are various methods of deriving TOA spectral radiance from a Landsat satellite image. However, in this study, a method given in Landsat 8 User handbook was used (USGS, 2016) following equation (8) below. Table 3.3 provides constants for Landsat 8 image metadata file that are used for calculation of TOA and brightness temperature (BT).

$$TOA(L_\lambda) = M_L * Q_{cal} + A_L \quad \ldots\ldots (8)$$

Where TOA is top of atmospheric spectral radiance (Watts/ (m² ·sr·μm), M_L is band-specific multiplicative rescaling factor (Table 3.3), Q_{cal} is Quantized and calibrated standard product pixel values (DN) corresponds to band 10 and A_L is band specific additive rescaling factor.

Table 3.3: Landsat 8 image metadata file downloaded for the city of Johannesburg (Rosebank and Soweto) for the calculation of brightness temperature (BT) and top of atmospheric (TOA).

Variable	Description	Value
K_1	Thermal conversion constant	774.8853
K_2	Thermal conversion constant	1321.0789
M_L	band-specific multiplicative rescaling factor	0.0003342
A_L	band specific additive rescaling	0.1

3.9.2. Conversion of TOA to BT

After obtaining TOA spectral reflectance radiance, brightness temperature was calculated according to equation (8) **(**Chander and Markham, 2003; Jiménez-Muñoz *et al*., 2014; USGS, 2016). Therefore, metadata file of Landsat 8 image (from Table 3.3 above) was used for the conversion of TOA to BT as follows:

$$BT = \frac{K2}{Ln\left(\frac{K1}{L\lambda}+1\right)} \quad \ldots\ldots (9)$$

Where BT is brightness temperature (Kelvin), K_1 and K_2 are band 10 thermal conversion constants for Landsat 8 TIRS metadata file expressed in Kelvin (Table 3.3), *Ln* is natural logarithm and L_λ is top of atmosphere (Watts/ m^2 * sr * μm) calculated in equation (8).

3.9.3. Converting BT from Kelvin to degrees Celsius

According to Paul and Ziaul (2017), 0 ^{o}C is equivalent to 273.15 Kelvin, the units of BT obtained in equation (9) are in Kelvin, hence it is necessary to convert the units to degree Celsius by subtracting 273.15 from the answer. Therefore, equation (9a) was derived from equation (9) as follows:

$$BT = \frac{K2}{Ln\left(\frac{K1}{L\lambda}+1\right)} - 273.15 \quad \text{.....9(a)}$$

3.9.4. Normalized Difference Vegetation Index (NDVI) calculation

The Normalized difference vegetation index is a measure of vegetation cover (Rouse *et al*., 1974) and it is important for the analysis of biomass or greenness of an area (Ogunode and Akombelwa, 2017). The NDVI values for each pixel of the study areas images were calculated using band 4 and 5 of the Landsat 8 satellite image (Rouse *et al*., 1974). Low values of NDVI shows areas with less vegetation cover and higher values indicates densely vegetated areas. The NDVI values lie between -1 and +1. Alfraihat *et al*. (2016), stated that NDVI calculation is important for better understanding of vegetation patterns of urban cities and deriving land surface emissivity. Therefore, in this study calculation of NDVI and Pv was important for estimation of the proportion of vegetation cover (Pv) and land surface emissivity in equations (11) and (12) respectively. The NDVI of the Landsat 8 satellite image was calculated as follows:

$$NDVIi = \frac{NIRi - Redi}{NIRi + Redi}$$

.....(10)

Where NDVI is normalized difference vegetation index; NIR is near infrared band; Red is Red band; i is the pixel position in the scene (R = 4 and NIR = 5 for Landsat 8 data).

3.9.5. Calculation of the proportion of vegetation (P_v)

The P_v was derived from NDVI values obtained in equation (10) following the equation by Carlson and Ripley (1997). P_v can also be termed fractional vegetation cover (FVC). Areas of high vegetation have P_v values of 1 and bare soils have P_v values of 0. Therefore, P_v was calculated from NDVI based on equation (10).

$$P_v = \left(\frac{NDVI - NDVI_{min}}{NDVI_{max} - NDVI_{min}}\right)^2 \quad \text{.....(11)}$$

Where P_v is the proportion of vegetation, $\mathrm{NDVI}_{\max}$, $\mathrm{NDVI}_{\min}$ and NDVI were obtained from Landsat 8-pixel values.

3.9.6. Calculation of Land surface emissivity (ε)

Land surface emissivity refers to a percentage of radiance emitted by body temperature and the amount of the radiance emitted by a black body at the same temperature (Zhao-Liang *et al*., 2013). Therefore, land surface emissivity was obtained from the P_v layer and this was further used to estimate LST in equation (13). The land surface emissivity was calculated mathematically based on equation (12):

$$\varepsilon = 0.004 * P_v + 0.986 \quad \text{.....(12)}$$

Where **ε** is land surface emissivity and P_v is the proportion of vegetation.

3.9.7. Calculation of Land surface temperature

Finally, the land surface temperature of the whole image was calculated following an equation by Stathopoulou and Cartalis (2007) using the band 10 brightness temperature (BT) and land surface emissivity (ε). Through performing extraction by mask function in Arc Map 10.5, LST maps of Rosebank and Soweto areas were obtained. LST was further re-classified into five classes in Table 3.4 based on a method adapted from Sun *et al*. (2012). This classification was selected since the LST ranges were similar to those observations obtained in the present study and interpretation based on more classes was better as opposed to using two class ranges (High and Low). Also, Jenks natural break classification method was used in this research since it gives the best arrangement of values into classes (Sun *et al*., 2012) and this was performed in ArcGIS 10.5.

$$\mathrm{LST} = \frac{\mathrm{BT}}{(1+[(\frac{\lambda BT}{\rho})ln\varepsilon])} \quad \text{.....(13)}$$

Where LST is land surface temperature (°C), BT is the brightness temperature (°C), λ is an average wavelength of band 10, ρ = 1.438 × 10^{-2} mk, ln is natural logarithm and ε is the land surface emissivity calculated in equation (12).

Table 3.4: Description of Land surface temperature (LST) classes for Rosebank and Soweto areas in Johannesburg.

Type	Range (^{O}C)	Description
LLA	-4- 10	Very low LST areas
LA	10- 15	Low LST areas
NA	15- 20	Normal LST areas
HA	20- 25	High LST areas
HHA	25- 31	Very high LST areas

3.10. Normalized Difference Built-up Index (NDBI) calculation

To identify all built-up areas of Rosebank and Soweto suburbs Landsat 8 satellite image, NDBI was calculated following a method suggested by Zhang (2006). The NDBI has been widely used for mapping, deriving and extraction of information related to built-up areas while NDVI is as an indicator of greenness (Ahmed, 2018). Normalized Difference Built-up Index values lie between -1 and +1, low NDBI represent water bodies and larger positive NDBI values represent built-up or impervious concrete surfaces. The derived Normalized Difference Built-up Index values were further used to determine correlation coefficient (r) between NDBI vs. LST and NDVI vs. NDBI and to give information to urban development planners to facilitate protection of urban environments. In order to calculate NDBI, equation (14) was used:

$$NDBI = \frac{MIR-NIR}{MIR+NIR}$$

……...(14)

Where NDBI is normalized difference built-up index, NIR is near infrared band 5 and MIR is middle infrared band 6 of Landsat 8 data.

3.11. Surface radiation estimation

Surface radiation refers to the amount of energy exchange through the reflection of electromagnetic waves which transport energy from reflecting object (Orimoloye *et al*., 2018). Despite, sunlight being an essential component for human life excess sunlight can be harmful and detrimental (WHO, 2002). Exposure to excessive solar radiation can lead to acute and chronic health problems that include sunburn, heat stroke, eye cataracts, premature wrinkling and skin cancers and heart problems (WHO, 2002; Orimoloye *et al*., 2018). The

Global solar ultraviolet (UV) Index developed by WHO in 1994 (amended later in 2002) classify solar radiation into categories and corresponding health effect. According to WHO (2002), Global solar UVI refers to the level of solar radiation at the Earth's surface and its values lie between 1 and 10 but in some places, this can reach 11+ (the highest class of global solar UVI). Higher values of UVI means a higher probability of skin and eye damage and shorter time for damage to occur. Therefore, UVI was estimated for Rosebank and Soweto suburbs to explain the effects of solar radiation on the health of city dwellers living in the two suburbs. After obtaining the raster file of radiation power (P), it was reclassified into five classes using Arc Map 10.5. Table 3.5 gives the thresholds of UVI and likely health implications of solar radiation (WHO, 2002). Solar radiation power was calculated following equation (15):

$$P = \varepsilon \sigma A T^4 \quad \ldots\ldots \quad (15)$$

Where P is radiation power, ε is the land surface emissivity, σ is Stefan-Boltzmann constant (5.67×10^{-8} W/ m^2K^4), T is land surface temperature (Kelvin/ ^oC) and A is Surface area ($4\pi r^2$). Following Roy *et al*. (2016), r was taken to be 6371 km equivalence to Earth's radius and π is constant (3.142).

Table 3.5: The Global solar ultraviolet (UV) Index threshold used for solar radiation classification for Rosebank and Soweto areas.

Index number	Exposure category	Colour code	Health effect
1- 2	Low	green	normal
3- 5	Moderate	yellow	Fatigue possible with prolonged exposure
6- 7	High	orange	Heat cramps, heat exhaustion with prolonged exposure
8- 10	Very high	red	Skin disease and heat stroke and
11+	Extreme	purple	Skin cancer and cardiovascular diseases

3.12. The Urban Thermal Field Variance Index (UTFVI)

Land surface temperature has been widely considered for urban heat analysis. However, some scholars have further utilized the urban thermal field variance index (UTFVI) to analyse the effects of urban heat island (Zhang, 2006; dos Santos *et al*., 2018; Alfraihat *et al*., 2016). The

UTFVI is an index that quantifies the effects of urban heat island on urban dwellers' quality of life (Zhang, 2006; Alfraihat *et al*., 2016). It was necessary to link the effects of urban heat island with UTFVI to evaluate the ecological effects of UHI in relation to urban people's quality of life in the two suburbs. To evaluate the effects of UHI intensity on the ecological aspects of Rosebank and Soweto suburbs, UTFVI was calculated (Zhang, 2006). The UTFVI was re-classified into six categories and a description of each class threshold is shown (Table 3.6) (Zhang, 2006). After obtaining the UTFVI raster file, using ArcMap 10.5 reclassify tool the six classes were derived. The larger the LST value, the greater is the heat effect (Liu and Zhang, 2011). The urban thermal field variance index was calculated as follows;

$$UTFVI = \frac{T_s - T_m}{T_s} \quad \text{.....(16)}$$

Where UTFVI is urban thermal field variance index, T_s is Land surface temperature (K/ ^{o}C) and T_m is mean LST (K/ ^{o}C) of the whole image.

Table 3.6: Ecological evaluation index threshold values for classifying urban heat island phenomenon in Rosebank and Soweto areas in Johannesburg.

Urban thermal field variance index	Urban Heat Island Phenomenon	Ecological evaluation Index
< 0	None	Excellent
0- 0.005	Weak	Good
0.005- 0.01	Middle	Normal
0.01- 0.015	Strong	Bad
0.015- 0.02	Stronger	Worse
> 0.02	Strongest	Worst

3.13. Statistical Analysis

Pearson correlation

To determine the influence of vegetated areas and built-up areas on urban heat island effect, Pearson correlation was performed among three variables (NDBI, NDVI and LST), this was done using Ms Excel 2016 and a correlation matrix was established for quantitative evaluation. Each index was classified into ten classes and class values were used to perform

correlation analysis. Prior to performing the Pearson correlation, two assumptions were considered in this study;

- LST values are positively correlated with NDBI values.
- LST values are negatively correlated with NDVI values.

CHAPTER 4: RESULTS

4.1. Plant biomass estimation using allometric equation and remote sensing

A total of 120 trees comprised of *Jacaranda mimosifolia* (58) and *Platanus acerifolia* (62) were recorded and ground control points were taken in Rosebank suburb and the amount of carbon content in AGB was estimated. Pearson correlation was performed among estimated field AGB, NDVI and band values to determine the best equation to extract biomass from SPOT 6 satellite images. There was weak correlation between field estimated AGB and band 1 ($r^2 = 0.02$); AGB and band 2 ($r^2 = 0.00$); AGB and band 3 ($r^2 = 0.01$; AGB and band 4 ($r^2 = 0.11$). However, correlation results showed a strong positive relationship between AGB and NDVI values ($r^2 = 0.93$) (Figure 4.1). Therefore, in this study, the equation with the highest r^2 value was used to obtain AGB from SPOT 6 satellite images for Rosebank suburb (Figure 4.1). The same equation was also used to derive total AGB for the Soweto area (Table 4.1).

Results of biomass extraction based on remote sensing calculation showed that there was more total AGB in Soweto compared to Rosebank (Figure 4.2). However, Rosebank showed a higher greenness index of 0.86 compared to Soweto with 0.14 (Table 4.1). This shows that there was more tree cover in Rosebank than Soweto suburb as indicated by the combined total percentage of the four classes (*Jacaranda mimosifolia*, *Platanus acerifolia* and Other vegetation and Grasses) considered for greenness index calculation. Figure 4.3 shows the carbon content for the two areas and it was clearly indicated that the white areas on the maps with no biomass were the same areas with negative NDVI and High NDBI values.

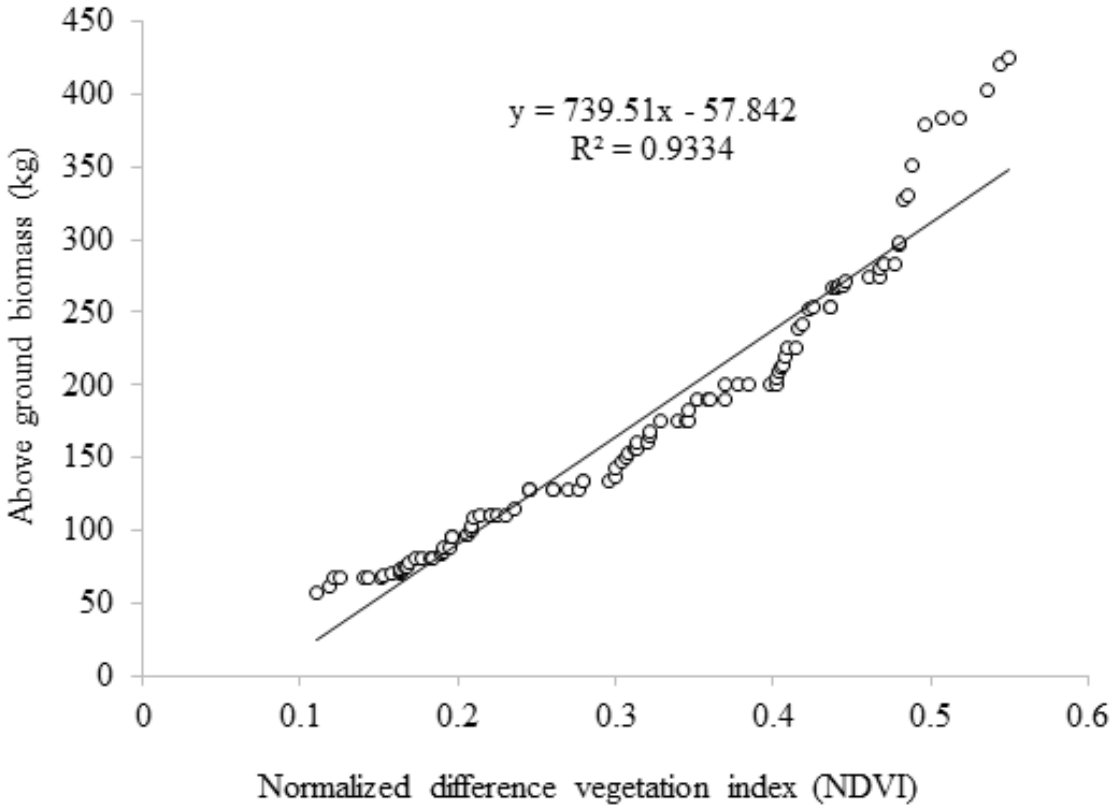


Figure 4.1: Correlation relationship between estimated above ground biomass and normalized difference vegetation index (NDVI).

Table 4.1: Carbon content in above ground biomass (AGB) and greenness index of Rosebank and Soweto suburbs in Johannesburg.

City	Biomass (ton)	Carbon (ton)	Greenness index
Rosebank	113179.03	50930.56	0.86
Soweto	504399.97	226979.99	0.14

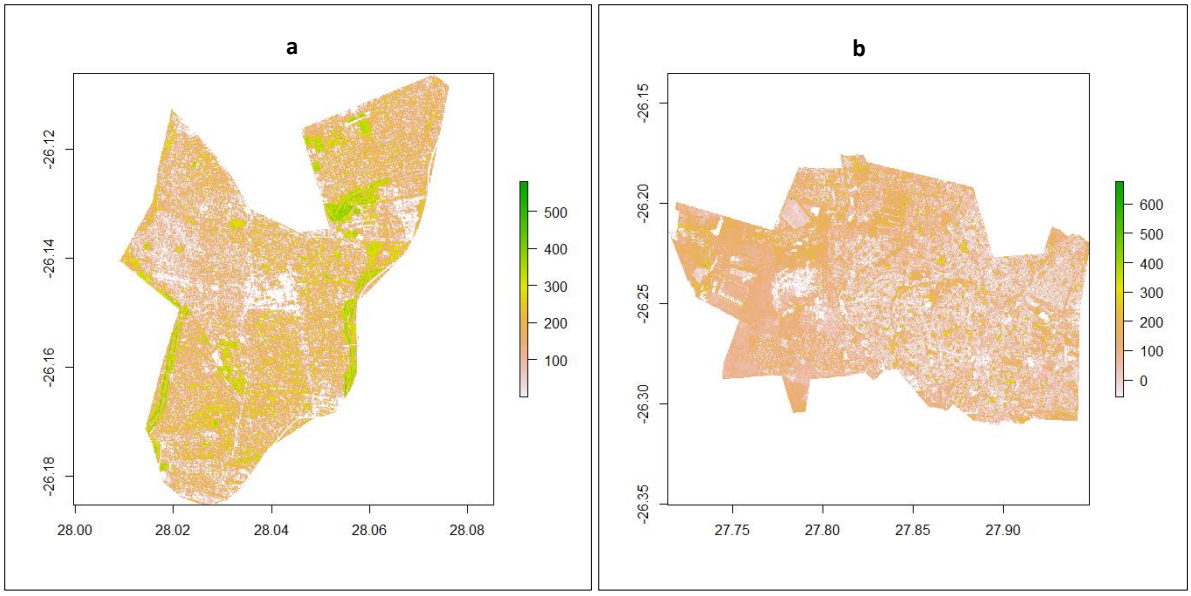


Figure 4.2: Maps of above ground biomass for (a) Rosebank and (b) Soweto areas in the City of Johannesburg derived from SPOT 6 satellite image. N.B. Dark green- high biomass, yellow- medium biomass, grey- low biomass, white- no biomass.

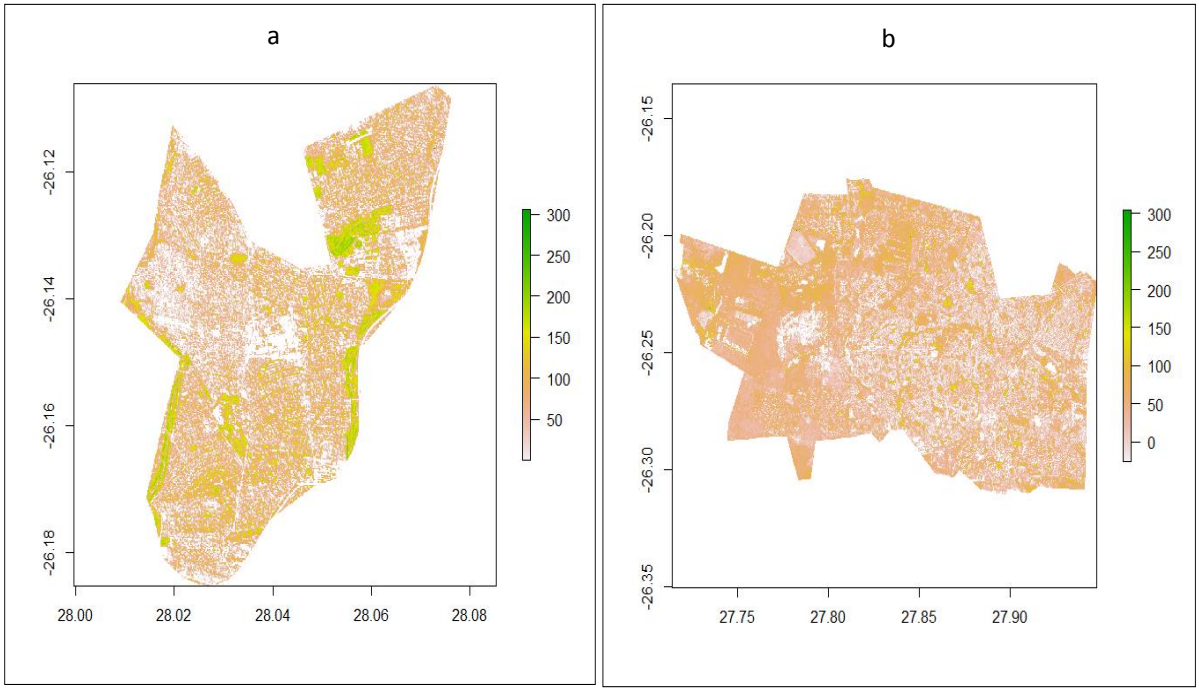


Figure 4.3: Maps of carbon content sequestered in plant biomass for (a) Rosebank and (b) Soweto areas in the City of Johannesburg. N.B. Dark green- high carbon, yellow- medium carbon, grey- low carbon, white- no carbon.

4.1.1. Random forest classification

The largest area (17.00 km^2) of Rosebank was occupied by 'other vegetation' class and this shows that besides the dominant London plane and Jacaranda species the contribution of other tree species is significant in regulating land surface temperature of the area. The class representing swimming pool had the lowest area coverage (0.04 km^2) followed by the bare soil class (Table 4.2). In Soweto the results revealed that the bare soil class occupied the largest area with 58.01 %, followed by brown built-up (22.36 %) and lastly swimming pool (0.14 %) (Table 4.2). This showed that bare soil area in Soweto is much larger compared to Rosebank (1.58 %). There was a larger area covered by water in Rosebank (3.29 %) compared to Soweto (2.67 %) suburb and this is shown by blue colour on the two maps (Figure 4.4). Also, Rosebank suburb had a higher proportion of grasses (3.05 %) compared to that of Soweto (Table 4.2) which is shown by the light green colour on the Rosebank map (Figure 4.4).

Table 4.2: Results of Random Forest classification of land cover classes of Rosebank and Soweto areas in Johannesburg.

Land cover class	Rosebank		Soweto	
	Area (km^2)	Percentage (%)	Area (km^2)	Percentage (%)
Bare soil	0.48	1.58	130.4	58.01
Brown built up	1.30	4.28	50.27	22.36
Grasses	1.00	3.29	0.54	0.24
Jacaranda	2.08	6.84	0.33	0.15
London plane	6.00	19.74	10.47	4.66
Other vegetation	17.00	55.92	20.11	8.94
Swimming pool	0.04	0.13	0.32	0.14
Water	1.00	3.29	6.00	2.67
White built up	1.50	4.93	6.36	2.83
Total	30.40	100	224.80	100

4.1.2. Accuracy assessment

Results of Random Forest classification indicated that the model was more accurate in identifying all nine landcover classes. The overall accuracy was 96.59 % which implies strong agreement. Highest producer accuracy of 100 % was obtained for water and white

built-up classes and highest user accuracy was recorded for grasses class. However, the lowest producer accuracy of 92.29 was obtained for '*Other vegetation*' class while lowest User accuracy (89.32 %) was recorded for '*Other vegetation*' (Table 4.3). In addition, the RF classifier algorithm performed very well as indicated by the kappa coefficient of 0.96 (Table 4.3). Therefore, the model of Rosebank was used for classifying the Soweto image since there were no ground truthing points and the classified images are shown in Figure 4.4.

Table 4.3: Confusion matrix for Rosebank obtained from Random Forest classifier.

	BS	BBU	G	J	LP	OV	SP	W	WBU	Total	PA (%)
BS	928	7	0	0	1	0	0	0	0	936	99.15
BBU	7	353	0	0	0	0	0	0	0	360	98.06
G	0	0	2579	2	0	0	0	0	0	2581	99.92
J	0	0	0	1624	0	162	0	0	0	1768	90.92
LP	0	0	0	0	931	34	0	0	0	965	96.48
OV	0	0	0	105	32	1639	0	0	0	1776	92.29
SP	0	0	0	0	0	0	473	0	0	473	100
W	0	0	0	0	0	0	0	436	0	436	100
WBU	0	3	0	0	0	0	0	0	1023	1026	99.71
Total	935	363	2579	1731	964	1835	473	436	1023	10339	
UA (%)	99.25	97.25	100	93.82	96.58	89.32	100	100	100		
Overall Accuracy = 96.59 %					Kappa coefficient = 0.96						

(BS- Bare soils; BBU- brown built-up; G- grasses; Jacaranda; LP- London plane; SP- swimming pool; W- water; WBU- white built-up).

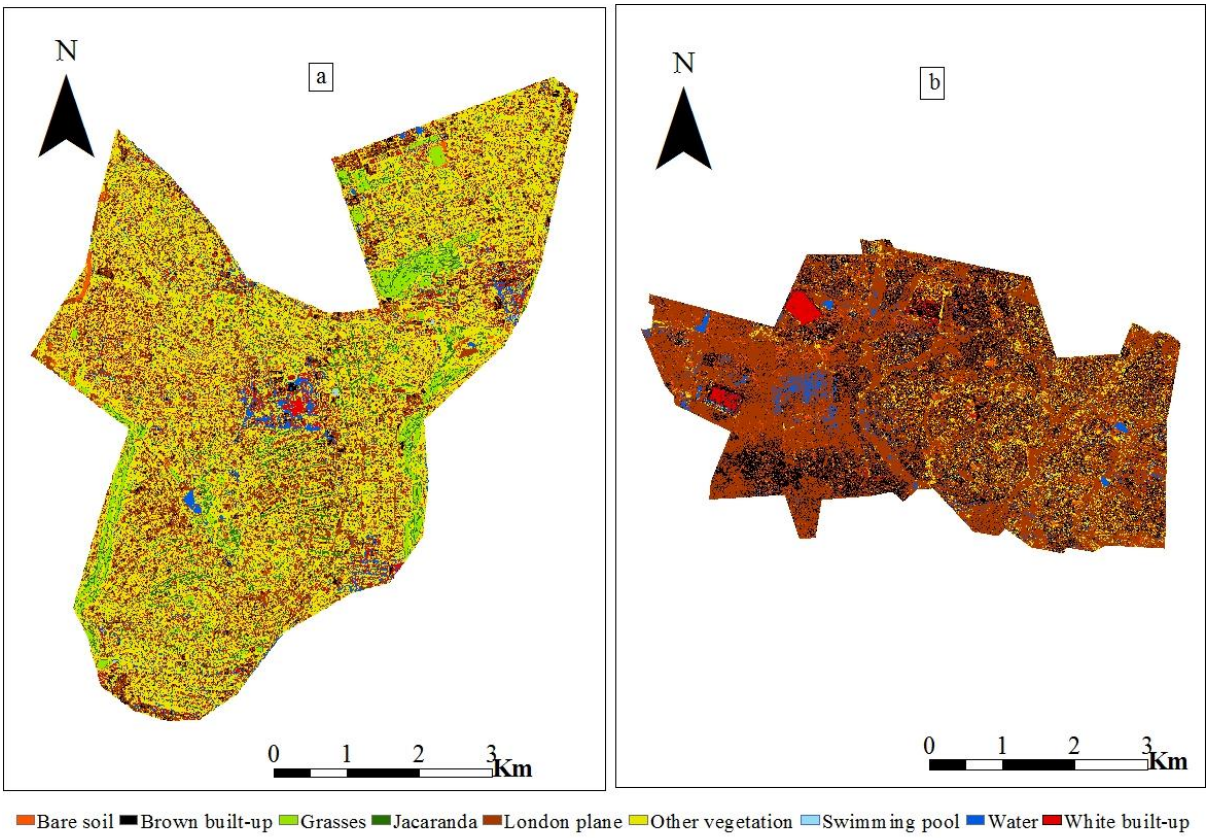


Figure 4.4: Classified SPOT 6 pan-sharpened images for land cover classes of (a) Rosebank and (b) Soweto, in Johannesburg.

4.2. Vegetation index

The Normalized Difference Vegetation Index (NDVI) maps of Soweto and Rosebank suburbs were generated from SPOT 6 pan-sharpened satellite images (Figure 4.5). The NDVI images produced were re-classified into four classes namely: low, moderate, high and very high-green quality (Figure 4.5). Both study areas had the same highest NDVI values being 0.999, while, the lowest NDVI values recorded were -0.999 and -0.997 for Rosebank and Soweto respectively. Water bodies exhibited low NDVI values and these areas are indicated by white colour on the two maps. In contrast, green vegetated areas exhibited high NDVI values and these are shown in dark green colour on the maps (Figure 4.5). Moderate green quality was the dominant NDVI class as indicated on the maps (Figure 4.5). The low green quality class was mostly dominated by surface water bodies and built up areas, thus had negative NDVI values. Figure 4.2 clearly shows that areas depicted as water (in blue colour) are the same areas that had low green quality (in white colour) (Figure 4.5). Overall, the NDVI values showed not much difference between the two study areas.

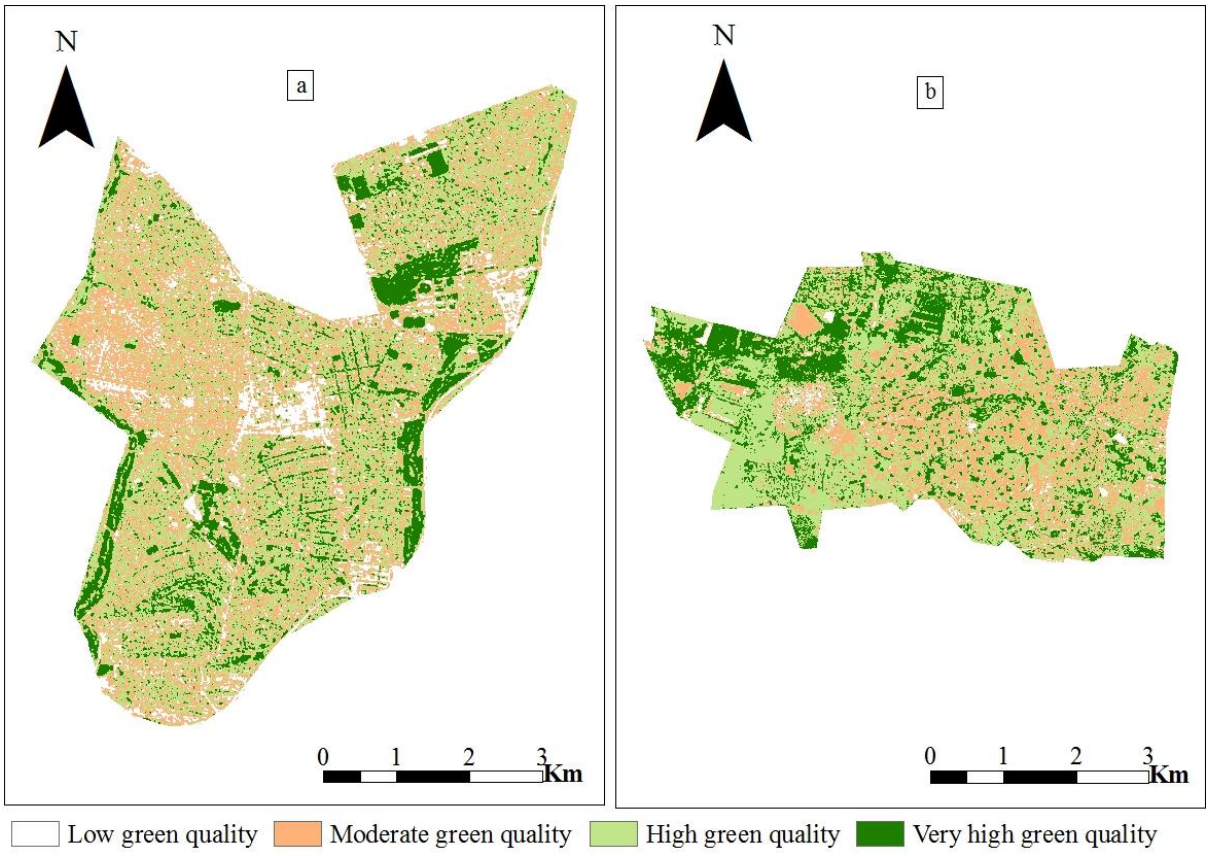


Figure 4.5: Normalized Difference Vegetation Index (NDVI) classification maps of Rosebank (a) and Soweto (b) areas, in Johannesburg derived from SPOT 6 data.

4.3. Urban heat island

The land surface temperature maps of Rosebank and Soweto study areas were derived from the Landsat 8 image as indicated below (Figure 4.6). The land surface temperature was re-classified into four classes as given in Table 4.4. Class of Very High LST areas was not represented since both study areas had LST values less than the designated class range, therefore it was not included (Figure 4.6). The highest LST of 23.60 ^{o}C was obtained in Soweto compared to 21.12 ^{o}C for Rosebank suburb. The difference (2.48 ^{o}C) observed in LST between the two areas could be attributed to the higher vegetation cover in the less densely populated Rosebank than in Soweto areas. Less bare soils in Rosebank also contributed to low LST compared to Soweto with more bare soils, built up and less vegetated areas. Less bare soils in Rosebank also contributed to low LST compared to Soweto with more bare soils, built up and less vegetated areas. Low values of LST ranged from -4.49 ^{o}C to 0.55 ^{o}C for Rosebank and Soweto respectively. Also, the lowest land surface temperatures were obtained from surface water bodies. The highest land surface temperature was found in areas with lower NDVI and higher NDBI and the reverse was true for the lowest land surface

temperature values. Table 4.4 clearly shows that Soweto has higher LST compared to Rosebank in all the four classes. A greater proportion of Rosebank suburb falls in Low LST areas covering an area of 25.85 km^2 while Normal LST areas covered a total of 184.64 km^2 constituting 82.88 % of Soweto (Table 4.4). Also, the Soweto suburb had a higher percentage of areas with High LST compared to Rosebank suburb (Figure 4.6). From Figure 4.6 it can be observed that High LST areas and occurred in areas with high NDBI values (Figure 4.7) and this reveals a direct link of land surface temperature and built-up areas.

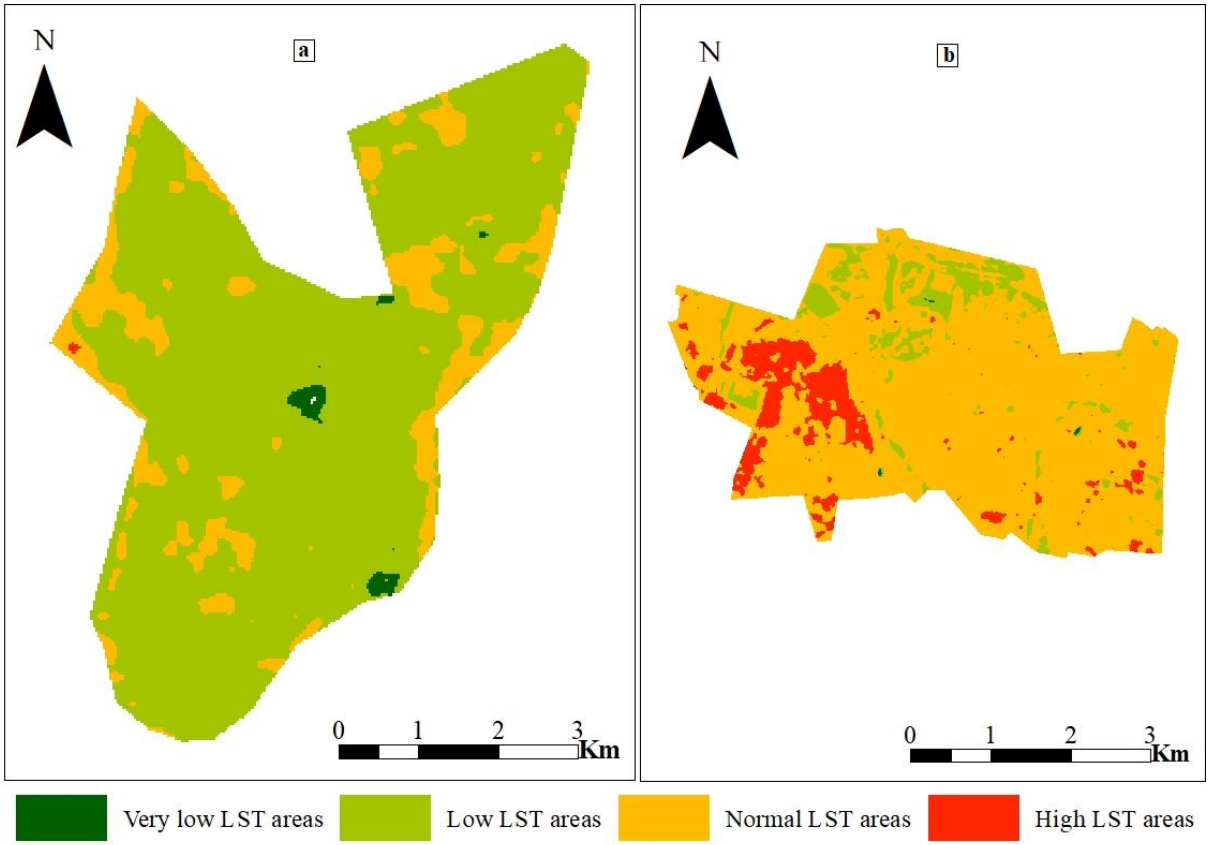


Figure 4.6: Land surface temperature maps of Rosebank (a) and Soweto (b) suburbs obtained from Landsat 8 data.

Table 4.4: Land surface temperature (LST) results of Rosebank and Soweto suburbs in Johannesburg derived from Landsat 8 data.

LST type	Range (°C)	Area (km^2)		Percentage (%)	
		Rosebank	Soweto	Rosebank	Soweto
VLA	-4-10	0.26	0.13	0.86	0.06
LA	10-15	25.85	19.09	85.03	8.57
NA	15-20	4.28	184.64	14.07	82.88
HA	20-25	0.01	20.92	0.05	9.39
Total		30.40	224.80	100	100

(VLA- very low LST areas; LA- low LST areas; NA- normal LST areas; HA- high LST areas)

Pearson correlation

The Pearson's correlation coefficient was performed to determine the relationship among NDVI, LST and NDBI derived from Landsat 8 images and the results are given in (Table 4.5). The correlation results showed a strong positive correlation between LST and NDBI values showing 0.92 and 0.98 for Rosebank and Soweto areas respectively. This indicates that as NDBI values increases, the LST also increases and "LST values are positively correlated with NDBI values" in section 3.13 was true. From Figure 4.7 it can be noted that areas with high NDBI were categorized as High LST values (Figure 4.6). However, there was a strong negative correlation between LST and NDVI values, highlighting that as NDVI increases, LST decreases (Table 4.5), thus "LST values are negatively correlated with NDVI values" in section 3.13 was true. Since NDVI is an indicator of vegetation cover, it means areas with higher NDVI values were associated with low land surface temperatures compared to low vegetated areas with high LST. Similarly, correlation analysis between NDVI and NDBI values showed a negative relationship for both study areas (Table 4.5). Overall, the Soweto suburb had the highest Pearson correlation coefficient values for all the indices compared to Rosebank.

Table 4.5: Results of Pearson correlation coefficient among Normalized Difference Built-up Index (NDBI), Normalized Difference Vegetation Index (NDVI) and Land Surface Temperature (LST) of Rosebank and Soweto suburbs in Johannesburg.

Variable	Rosebank	Soweto	Rosebank	Soweto	Rosebank	Soweto
	LST		NDVI		NDBI	
LST			-0.99	-0.91	0.92	0.98
NDVI	-0.99	-0.91			-0.90	-0.85
NDBI	0.92	0.98	-0.90	-0.85		

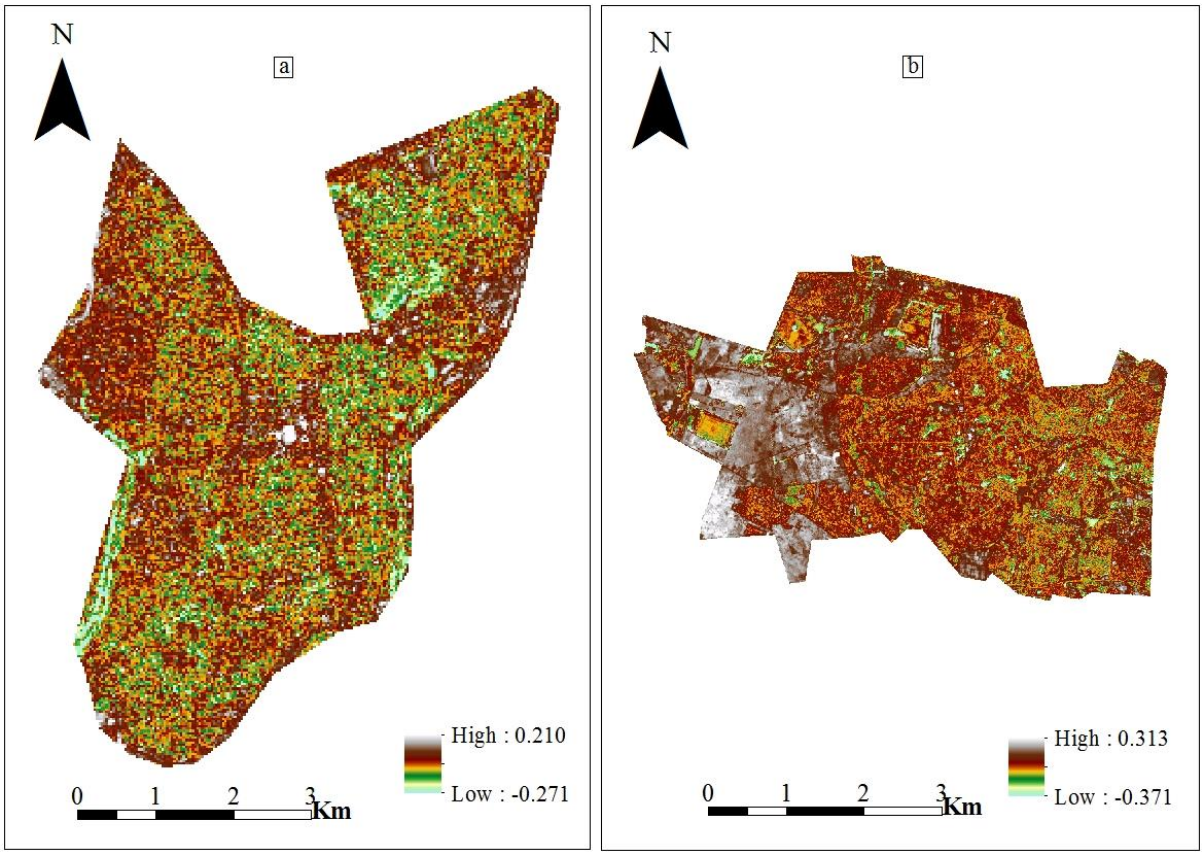


Figure 4.7: The maps of Normalized Difference Built-up Index of (a) Rosebank and (b) Soweto suburbs derived from Landsat 8 satellite data.

Ecological assessment of Rosebank and Soweto suburbs

The ecological pattern in Rosebank and Soweto suburbs were evaluated by calculating the Urban Thermal Field Variance Index (UTFVI) values. Various levels of Urban Heat Island pattern were observed in the two study areas (Table 4.6). A small area of Rosebank suburb (24.50 %) falls within Worse to Worst category highlighting evidence of UHI phenomenon.

Areas that were found to be in excellent, good and normal classes for Rosebank suburb also indicated to be areas with low NDBI values (Figure 4.7). The two maps clearly showed that all areas depicted as Bad, Worse and Worst (Figure 4.8) occurred in areas with high NDBI values and high UVI category (Figure 4.7 and Figure 4.8 respectively) in Soweto suburb indicating a case of UHI phenomenon in this area. Thus, people living in such areas are likely to suffer from urban heat island effects as a result of more LST contributing to increased solar radiation. Rosebank suburb recorded highest UTFVI in Bad zone compared to Soweto with highest UTFVI area coverage in Normal LST class although there was some evidence of severe impacts of UHI in Soweto than low-density Rosebank area. The ecological evaluation index of Rosebank in the Worse category was higher (4.68 %) compared to that of the Soweto area.

Table 4.6: Results of Urban Thermal Field Variance Index (UTFVI) coverage in Rosebank and Soweto suburbs in Johannesburg derived from Landsat 8 data.

UTFVI index	Ecological evaluation	Rosebank		Soweto	
		Area (km^2)	Percentage (%)	Area (km^2)	Percentage (%)
< 0	Excellent	0.06	0.20	4.53	2.02
0- 0.005	Good	1.03	3.38	22.95	10.20
0.005- 0.01	Normal	10.84	35.65	87.09	38.74
0.01- 0.015	Bad	11.03	36.28	68.20	30.34
0.015- 0.02	Worse	6.31	20.75	36.13	16.07
> 0.02	Worst	1.14	3.75	5.85	2.60
	Total	30.4	100	224.8	100

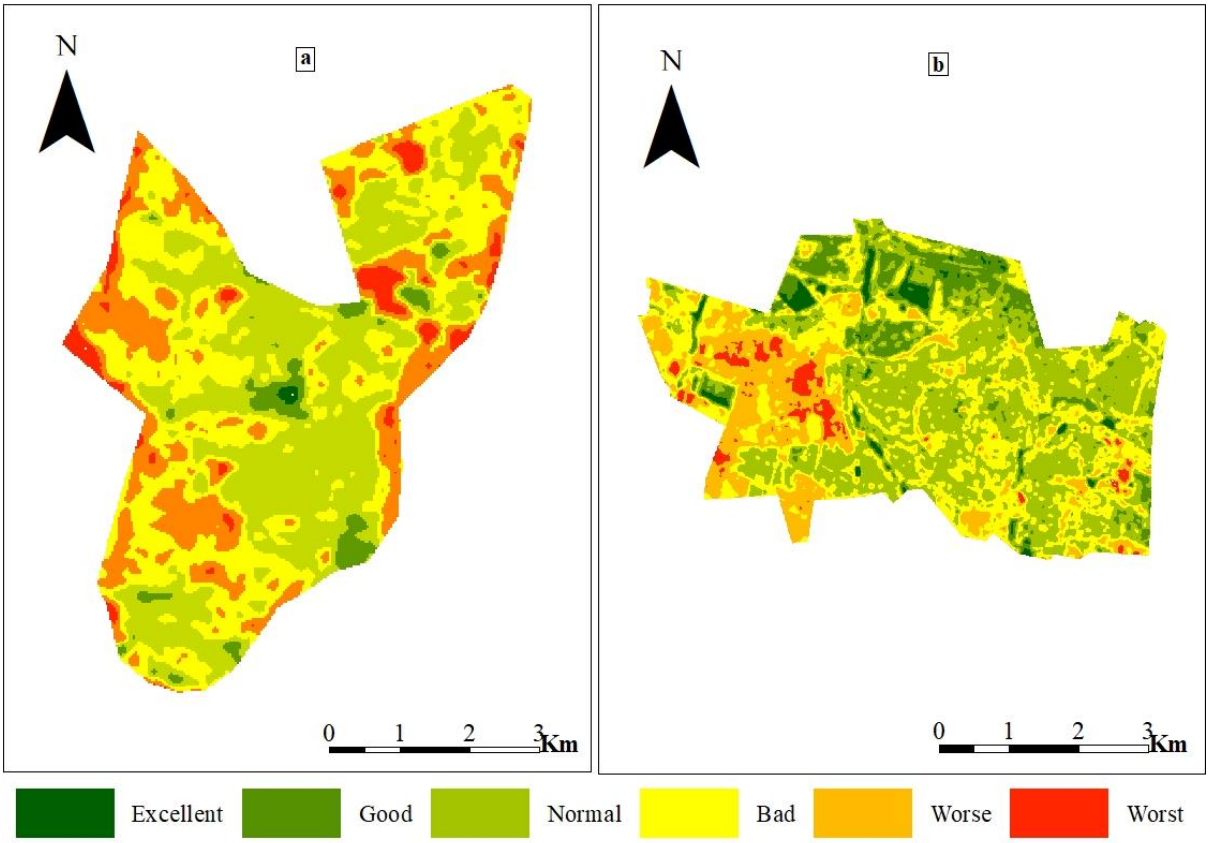


Figure 4.8: Ecological assessment of (a) Rosebank and (b) Soweto suburbs based on Urban Thermal Field Variance Index (UTFVI) in the City of Johannesburg.

Evaluation of Solar Radiation in relation to global solar Ultraviolet Index (UVI) in Rosebank and Soweto suburbs.

The spatial distribution of the effects of solar radiation based on analysis of Ultraviolet Index (UVI) for Soweto and Rosebank suburbs is shown in Figure 4.9 and the area coverage for each UVI class is shown in Table 4.7. In Rosebank the effect of solar radiation has fewer effects since 83.13 % of the total area falls within low to moderate exposure class. In contrast, Soweto suburb had 68.07 % of the total area falling in low to medium exposure category with the remaining area designated as high to very high exposure category (Table 4.6). About 11.15 % of the total Soweto area was highly affected by solar radiation compared to 1.77 % area in Rosebank suburb. Similarly, areas highlighted as high LST (Figure 4.6 above) were the same areas that had high solar UV radiation exposure. Soweto suburb had a larger proportion of area (20.77 %) with High UV compared to that of Rosebank (15.09 %) in the same category. For all the two study areas there was no evidence of 11+ class (Extreme) recorded and therefore, it was not represented on the maps and table.

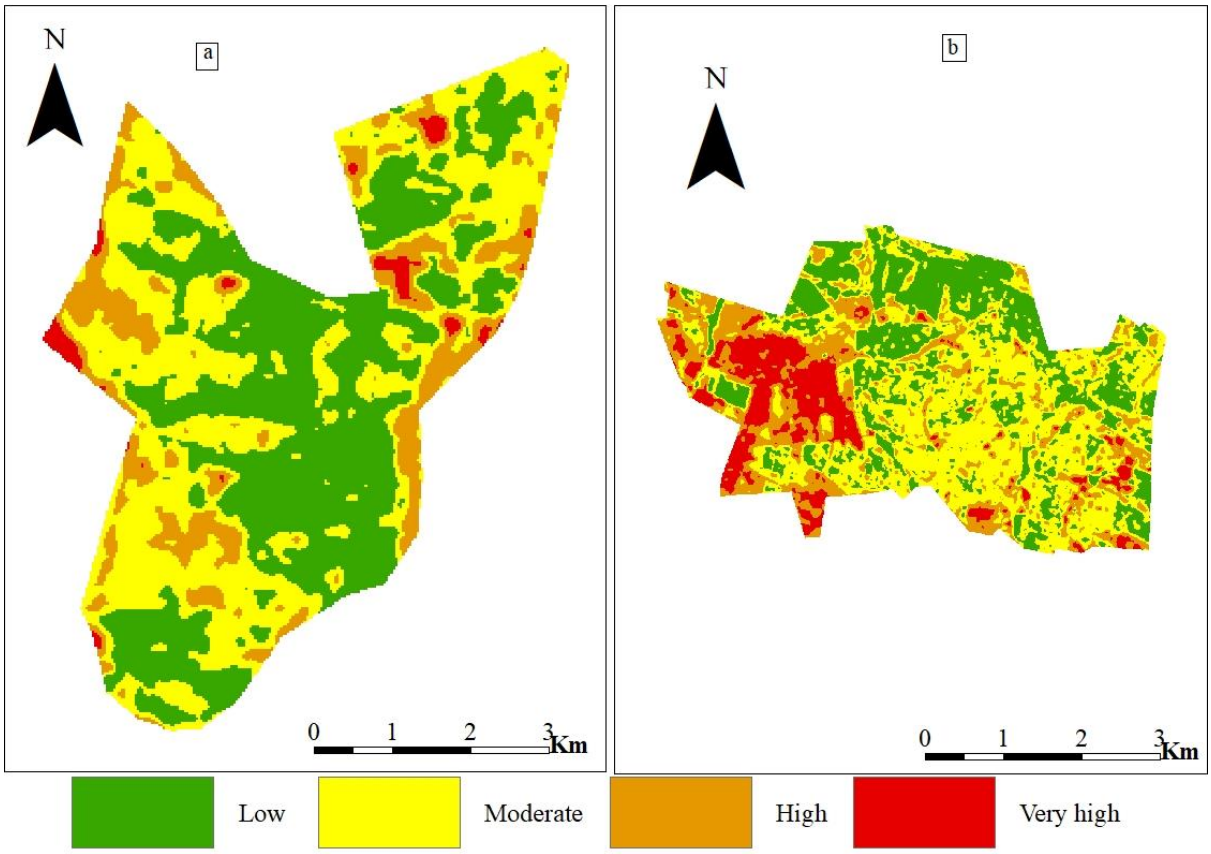


Figure 4.9: Maps showing extend of solar radiation exposure estimated from Global Solar Ultraviolet (UV) index in the suburbs of Johannesburg (a) Rosebank and (b) Soweto.

Table 4.7: Results of global solar Ultraviolet (UV) index analysis for Rosebank and Soweto suburbs in the city of Johannesburg.

Index number	Global solar UV	Rosebank		Soweto	
		Area (km^2)	Percentage (%)	Area (km^2)	Percentage (%)
1- 2	Low	12.89	42.37	58.87	26.18
3- 5	Moderate	12.40	40.76	94.19	41.89
6- 7	High	4.59	15.09	46.70	20.77
8- 10	Very high	0.54	1.77	25.08	11.15
	Total	30.4	100	224.8	100

CHAPTER 5: DISCUSSION AND CONCLUSIONS

This section mainly focused on the results interpretation and linkage with findings of other scholars and was structured based on the objectives stated below:

a) To measure plant biomass using allometric equations and SPOT 6 satellite imageries in the two urban environments of Johannesburg (Soweto and Rosebank).
b) To determine the vegetation index of Soweto and Rosebank for urban environment condition analysis using SPOT 6 data.
c) To compute an environmentally friendly greenness index based on a ratio between the total area of a city or suburb covered by green vs. the total area of a city.
d) To determine the urban heat island using thermal Landsat 8 data in Rosebank and Soweto as case study areas.

5.1. Biomass estimation and remote sensing

Estimating above ground biomass of urban street trees helps to determine the amount of carbon (from carbon dioxide) sequestered. Remote sensing could be the most feasible and sustainable method to estimate such biomass than traditional destructive sampling method which involves cutting down of street trees for sampling in urban areas. Based on a linear model of AGB and NDVI that had the highest correlation coefficient value ($r^2 = 0.93$), the total AGB of Rosebank and Soweto suburbs was estimated and the amount of stored carbon was also quantified.

The large biomass observed in the Soweto compared to that of Rosebank areas could be attributed to the differing size between the two study areas. Thus, the proportion of biomass was rather greater in Rosebank than in Soweto and therefore, the residents in the former suburb enjoy a better ecosystems service derived from urban greenness compared to Soweto residents. The carbon sequestration rates are, thus, higher in Rosebank than for the same area in Soweto. Since NDVI is an indicator of greenness, thus it was difficult to distinguish the contribution of grasses to total AGB of the two areas based on the current model (Figure 4.1). However, the highest NDVI values found in the two study areas could be a reflection that some areas had greener leaves, than others, which indicates high levels of photosynthesis. According to Gizachew *et al*. (2016), it is a challenge to distinguish the grass and tree above ground biomass based on a linear model with NDVI, but the model can calculate the total AGB of the area. Also, the intensity of grasses was not known when the satellite images were

taken, and this could have contributed to the high biomass of Soweto. However, in this study, no field data were taken to calculate the AGB of grasses.

5.2 Greenness Index

Rosebank suburb recorded a higher greenness index (0.86) compared to Soweto suburb (0.14) and this is an indication that Rosebank has more green areas which are very significant in regulating urban local climate and subsequently improving the people's health than in Soweto. The low value of greenness index of Soweto is evidential to the presence of 58.01 % of bare soil and 25.19 % of built-up areas in the suburb. The proportion of tree cover in Rosebank was higher (85.79 %) compared to that of Soweto areas which were 13.99 % and this explains why the greenness index was higher in Rosebank than in the latter. Also, most of the trees in Rosebank area were more matured and this could be the reason for its high biomass quantity since the age of trees has a direct relationship with AGB. A study by Hlatshwayo *et al*. (2019) observed that above ground biomass of trees was related to tree age. Their results showed that biomass of young plantation trees was 193.03 kg compared to that of matured plantation trees which was 670.43 kg. Therefore, in this study total, AGB of the two areas was successfully estimated from SPOT 6 pan-sharpened image using NDVI values.

5.3. Urban heat island

Quantification and analysis of urban greenness is important in evaluating the role of urban trees in carbon sequestration and regulating land surface temperature of urban environments. Remote sensing can evaluate the urban heat island phenomenon from Landsat satellite imagery by using thermal infrared sensors (TIRS). The LST was derived using Landsat 8 satellite image data for the two suburbs, Rosebank and Soweto. Land surface temperature (LST) analysis of Soweto and Rosebank was done and there was 2.48 ^{o}C difference between the two study areas. Soweto suburb had higher LST (23.60 ^{o}C) compared to Rosebank (21.12 ^{o}C) which could be attributed by the relatively large built-up areas available and the high population density (6357 people per km^2) in this suburb. Similarly, Rosebank suburb had a larger percentage of 76.43 % of Low LST areas compared to that of Soweto which suggests the influence of the vast tree cover in the area that promotes evaporative cooling. However, with regards to High LST areas a larger proportion (9.34 %) was found in Soweto compared to that of Rosebank. Thus, this can be due to more bare soils and open spaces which are poor absorbers of solar radiation leading to higher land surface temperatures. A study by Sun *et al*. (2012) revealed that the ratio of an area cover of similar LST classes was between 12.80 %

and 29.59 %. However, comparing these results with the present study it can be noted that those very Low LST areas of Soweto and Rosebank were lower (11.89 %). Shekhar and Kumar (2014) asserted that the expansion of cities accelerates land surface temperature through conversion of open green spaces and vegetation into residential housing, industrial sites and roads. Similarly, city expansion results in cutting down of trees to pave way for infrastructure development and this result in less biomass (reduced carbon sequestration) and increased LST (Buyadi *et al*., 2014). Soweto is known for its historical legacy as an informal settlement allocated for the local people by the apartheid regime (Crankshaw *et al*., 2000). It did not have a formal urban city plan such as boulevards and street trees. It is crowded with little or not enough spaces for garden trees (Crankshaw *et al*., 2000).

Present findings agree with the observation of Kaplan *et al*. (2018) of high urban heat island in high-density populated areas. In addition, Abutaleb *et al*. (2015) observed similar results of increased LST in populated high-density urban areas. Their results indicated that due to loss of vegetation cover and expansion of suburban areas the UHI increased by 4 km^2 in a period of four years. They also indicated that UHI values (0.85 ^oC - 2.7 ^oC) above mean land surface temperature was recorded in QesmMisr Al-Qadima and Cairo Egypt, highly populated settlements. The current population density of Soweto and Rosebank is recorded as 6357 people per km^2) and 1300 people per km^2, respectively, showing the massive demand for decent accommodation in the latter which potentially exacerbate the UHI condition failing to redesign and plant this suburb. Currently, Soweto has a high population density (6357 people per km^2) compared to Rosebank (1300 people per km^2) and this gives rise to an increase in demand for decent accommodation. In a different study conducted in the city of Chicago, USA, Alfraihat *et al*. (2016) found that the number of settlements influences the impact of build-up areas on land surface temperature. Their results revealed that low population density areas with more green spaces had lower LST compared to areas with high population density and less green spaces. The main findings of their results were high LST (> 38 ^oC) in industrial and high-density areas and low LST (29 - 32 ^oC) in vegetated areas, woodlands, green space and parks. Therefore, their results agree with the current findings of this study since higher LST were found in Soweto than in the Rosebank area.

Despite the greening Soweto initiative of 2006 by Johannesburg City Parks, the LST still remain higher compared to Rosebank suburb. The greater built-up areas (25.19 %) and bare soils (rocks and sand) (58.01 %) in Soweto compared to that of Rosebank is believed to be

the reason for such spikes in LST in Soweto. In addition, matured trees reduce the effects of urban heat island through evaporative cooling effect (Buyadi *et al*., 2014) and can sequester more carbon than smaller trees (Nowak *et al*., 2007). This can be attributed to more built-up areas (25.19 %) and a greater percentage of bare soils (rocks or sand) (58.01 %) in Soweto compared to that of Rosebank. In addition, matured trees reduce the effects of urban heat island through cooling (Buyadi *et al*., 2014) and can sequester more carbon than smaller trees (Nowak *et al*., 2007). Thus, it is not surprising that a high density of larger trees in Rosebank has a detrimental effect on the LST which is lower than that of Soweto. This confirms the vital role that the proportion of vegetation cover to built-up areas play in LST in an urban environment and the urban quality of life.

Other factors like landscape composition and local meteorological conditions can also influence the LST of an area (Ogunode and Akombelwa (2017). The LST ranges of the two study areas agree with results of Ogunode and Akombelwa (2017) who observed temperature ranges of 13 - 23 ^{o}C in Durban city center and 18 - 23 ^{o}C in well-populated areas. Vegetation cover of Rosebank was more pronounced compared to Soweto suburb and most of these trees were grown since the 19th century and thus the trees are more matured. Therefore, a clear distinction between LST of the two study areas was drawn with Soweto (high density) suburb having higher LST compared to Rosebank which has more street trees and relatively lower population density.

Ecological assessment of Rosebank and Soweto suburbs

The analysis of Urban Thermal Field Variance Index (UTFVI) showed that 2.60 % of Soweto lies in the Worst zone compared to Rosebank with 1.14 % which suggests the residents are subjected to more thermal discomfort compared to other residents in other UTFVI zones. This can be attributed to the presence of large bare soils and many built-up areas (tarred and concrete impervious surfaces) in Soweto and for Rosebank, this can be explained by the presence of huge tree cover in most of these areas that shade the streets and affects the LST. Also, the areas designated as Worst ecological evaluation index (Strongest urban heat island) were the same areas that had high NDBI and LST with low NDVI values. Despite some areas showing the strongest effect of urban heat island in both study areas, some areas that had high NDVI and low NDBI values were classified as 'Excellent' ecological evaluation index class. For example, in Soweto areas with Excellent ecological evaluation found to be closer to

water sources like rivers and reclaimed slime dams where tree cover was high. This supports the negative role of cooling by tree cover in reducing urban heat island effects.

Liu and Zhang (2011) used the same method of UTFVI analysis to assess the urban heat island effect in Hong Kong city, China. Their results revealed that Excellent ecological evaluation index was found in areas with high NDVI and low NDBI and LST areas while the Worst ecological index was found to be associated with areas of high LST and NDBI and low NDVI values. A study by dos Santos *et al*. (2018), revealed that highly populated urban built-up areas contribute to the degradation of the environment with ecological evaluation index in Worst zone. Kibert (2012) highlighted that the strategy of urbanism (promoting green buildings or planting of green plants on rooftops) can help lessen land surface temperature. However, due to the high population density of Soweto and lack of proper city design, it is complicated to implement greening initiatives to reduce land surface temperature. Rosebank suburb is relatively less congested compared to Soweto, it is therefore, ideal for the implementation of greening strategy since the street walkways or boulevards have extra space.

Analysis of Global Solar Ultraviolet (UV) index of Rosebank and Soweto suburbs.

The Global solar ultraviolet index plays a significant as a communication tool for raising public awareness and informing people to consider using protective measures in the event of exposure elevated levels of solar radiation. The present analysis of the effects of solar radiation based on the estimation of Global solar ultraviolet index using Landsat 8 satellite data revealed a clear distinction between Rosebank and Soweto areas. Kerr and Fioletov (2008) asserted that cloud cover reduces the quantity of solar ultraviolet radiation. The present study, however, showed the actual reality of the two suburbs in relation to proportions of tree cover to built-up and other urban characteristics and their direct impact on solar UV radiation, since the Landsat image had low cloud cover. It indicates that residents of Soweto suburb are at more risk of prolonged exposure to solar radiation compared to residents of Rosebank suburb. High exposure to solar radiation may lead to chronic health problems like skin cancers, eye cataracts and immune effects (WHO, 2002). However, no case-specific incidence was investigated in this study.

The results in Soweto suburb indicated that Very high exposure category (8-10) had a higher proportion (9.38 %) of affected areas compared to that of Rosebank. Similar, observation of

Global solar UV index of Very High exposure (8-10) category was reported by Orimoloye *et al*. (2018) from their study conducted in East London, South Africa. Their results showed that residents of East London area are at risk to effects of UV radiation exposure from the sun. This also reflects that the UHI phenomenon is a reality in urban areas of South Africa. Since Soweto residents are at more vulnerable to excessive exposure of UV radiation, there is a need for public awareness programs and encouragement on use of protective measures to reduce further damage (WHO, 2002). Some of the preventive methods that help reduce the effects of UV exposure include wearing sun hats, proper clothing, wearing sunglasses and correct use of sunscreens (WHO, 2002).

5.4. Conclusions

This study investigated the greenness index of the city of Johannesburg to determine its environmental suitability for its inhabitants. The study area was based on two suburbs as a case study. These were the affluent suburb of Rosebank and the informal Township of Soweto south of Johannesburg and the following conclusions were drawn:

The AGB and carbon content of Rosebank and Soweto areas were successfully derived from SPOT 6 image and higher AGB was found in Soweto (504399.97 tons) compared to that of Rosebank (113179.03tons). The NDVI proved to be a better predictor variable of total AGB than SPOT 6 bands. However, Rosebank had a higher greenness index value of 0.82 while that of Soweto was 0.14. Therefore, the residents of Rosebank area benefit more from greenness through better health and environmental air quality compared to those in Soweto.

The Land surface temperature was successfully retrieved from Landsat 8 TM satellite data and the distribution shows that Soweto was hotter (2.48 ^{o}C) compared to that of Rosebank suburb. Results of Pearson correlation coefficient among Normalized Difference Built-up Index (NDBI), Normalized Difference Vegetation Index (NDVI) and Land surface temperature (LST) values, showed that vegetation cover reduces the effects of urban heat islands while built-up areas increase such effects. Therefore, it is significant for urban planners to come up with measures that promote vegetation cover in urban centres especially in highly populated areas like Soweto to reduce the effects of UHI for better environmental and living conditions.

In addition, analysis of ecological assessment using UTFVI, indicated that 3.75 % and 2.60 % of Rosebank and Soweto areas respectively were affected by the UHI phenomenon. This requires urban planners and policymakers to improve and redesign cities to accommodate more tree cover and other green spaces in urban environments.

Present findings revealed that 11.15 % of the Soweto area is affected by the urban heat island phenomenon compared to that of Rosebank (1.77 %). In Rosebank, there was a larger percentage area (42.37 %) of Low UV exposure compared to 26.18 % for the Soweto area. People staying in areas designated as high to very high UV exposure are likely to suffer from health problems; therefore, measures should be taken by responsible authorities to prevent such environmental effects.

5.5. Recommendations

City planners should improve the urban environment condition of Soweto to increase its greenness index to reduce the widening gap of tree cover between the affluent areas of the City of Johannesburg. This will also contribute to increasing of AGB and carbon sequestration in the Soweto area.

The remote sensing images used in this study were downloaded from the winter season Thus, further investigation is necessary for relation to seasonal variations and long-term land use change detection comparisons between the two study areas. In addition, further studies are required to compare Landsat 8 satellite data with field LST measurements to validate the accuracy of LST derived from satellite images.

REFERENCES

Abrams, M. 2000. The Advanced Spaceborne Thermal Emission and Reflection Radiometer (ASTER): data products for the high spatial resolution imager on NASA's Terra platform. *International Journal of Remote Sensing*, 21, pp.847-859.

Abutaleb, K., Ngie, A., Darwish, A., Ahmed, M., Arafat, S. and Ahmed, F. 2015. Assessment of Urban Heat Island Using Remotely Sensed Imagery over Greater Cairo, Egypt. *Advances in Remote Sensing*, 4, pp.35-47.

Adam, E. M., Mutanga, O., Rugege, D. and Ismail, R. 2012. "Discriminating the Papyrus Vegetation (*Cyperus Papyrus*) and its Co-Existent Species Using Random Forest and Hyperspectral Data Resampled to HYMAP." *International Journal of Remote Sensing*, 33(2), pp.552-569.

Adiri, Z., El Harti, A., Jellouli, A., Lhissou, R., Maacha, L., Azmi, M., Zouhair, M. and Bachaoui, E. M. 2017. Comparison of Landsat-8, ASTER and Sentinel 1 satellite remote sensing data in automatic lineaments extraction: A case study of SidiFlah-Bouskour inlier, Moroccan Anti Atlas. *Advances in Space Research*, 60, pp.2355-2367.

Ahmed, S. 2018. Assessment of urban heat islands and impact of climate change on socioeconomic over Suez Governorate using remote sensing and GIS techniques. *The Egyptian Journal of Remote Sensing and Space Science*, 21(1), pp.15-25.

Alfraihat, R., Mulugeta, G. and Gala T. S. 2016. Ecological Evaluation of Urban Heat Island in Chicago City, USA. *Journal of Atmospheric Pollution*, 4(1), pp.23-29.

Alhawiti, R. H. and Mitsova, D. 2016. Using landsat-8 data to explore the correlation between urban heat island and urban land uses. *International Journal of Research in Engineering and Technology*, 5(3), pp.457-466.

Anandababu, D., Purushothaman, B. M. and Suresh, B. S. 2018. Estimation of Land Surface Temperature using LANDSAT 8 Data. *International Journal of Advance Research, Ideas and Innovations in Technology*, 5(3), pp.457-466.

Avitabile, V., Baccini, A., Friedl, M. A. and Schmullius, C. 2012. Capabilities and limitations of Landsat and land cover for above ground woody biomass estimation of Uganda. *Remote Sensing of Environment*, 117, pp.366-380.

Bhandari, A. K., Kumara, A. and Singh, G. K. 2012. Feature Extraction using Normalized Difference Vegetation Index (NDVI): A Case Study of Jabalpur City. *Procedia Technology*, 6, pp.612-621.

Breiman, L. 2001. "Random Forests." *Machine Learning*, 45(1), pp.5-32.

Brown, S., Gillespie, A. R. and Lugo, A. E. 1989. Biomass Estimation Methods for Tropical Forests with Applications to Forest Inventory Data. *Forest Science*, 35, pp.881-902.

Buff, A. 2012. Johannesburg City Parks and Zoo Tree Management Strategy.

Buyadi, S. N. A., Mond, W. M. N. W. and Misni, A. 2014. *IOP Conference Series.: Earth Environmental Science,* 18, pp.1-7.

Carlson, T. N. and Ripley, D. A. 1997. On the relation between NDVI, fractional vegetation cover, and leaf area index. *Remote Sensing of Environment*, 62, pp.241-252.

Chander, G. and Markham, B. L. 2003. "Revised Landsat-5 TM radiometric calibration procedures, and post-calibration dynamic ranges," *IEEE Transactions in Geoscience Remote Sensing*, 41(11), pp.2674-2677.

Chave, J., Anadalo, C., Brown, S., Cairns, M., Chamber, J., Eamus, D., Folster, H., Fromard, F., Higuchi, N., Kira, T., Lescure, J. P., Nelson, B., Ogawa, H., Puig, H., Riera, B. and Yamakura, T. 2005. tree allometry and improved estimation of carbon stocks and balance in tropical forests. *Oecologia*, 145, pp.87-99.

Cilliers, J. and Cilliers. S. 2016. Planning for green infrastructure: Options for South African cities. South African Cities Network. Johannesburg, South Africa.

City of Johannesburg. 2013. We're living in an urban forest. Available at: https://joburg.org.za/index.php? [Accessed 15 April 2018].

Crankshaw, O., Gilbert, A. and Morris, A. 2000. 'Backyard Soweto'. *International Journal of Urban and Regional Research*, 24(4), pp.841-857.

Dos Santos, A. R., de Oliveira, F. S., da Silva, A. G., Gleriani, J. M., Gonçalves, W., Moreira, G.L., Silva, F.G., Branco, E. R. F., Moura, M. M., da Silva, G. R., Juvanhol, R. S., Barbosa de Souza, K., Ribeiro, C. A. A. S., Tebaldi de Queiroz, V., Costa, A.V., Lorenzon, A. S., Domingues, G. F., Marcatti, G. E., de Castro, N. L. M., Resende, R. T., Gonzales, D. E., Telles, L. A., Teixeira, T. R., dos Santos, G. M. A. D. A., Mota, P. H. S. 2018. Spatial and temporal distribution of urban heat islands. *Science of The Total Environment*, 605-606, pp.946-956.

Dube, T. and Mutanga, O. 2015. Investigating the robustness of the new Landsat-8 Operational Land Imager derived texture metrics in estimating plantation forest aboveground biomass in resource constrained areas. *Journal of Photogrammetry and Remote Sensing*, 108, pp.12-32.

Dudley, N. S. and Fownes, J. H. 1992. Preliminary biomass equations for eight species of fast-growing tropical trees. *Journal of Tropical Forest Science*, 5(1), pp.68-73.

Fung, T. and Siu, W. 2000. Environmental quality and its changes, an analysis using NDVI, *International Journal of Remote Sensing*, 21(5), pp.1011-1024.

Gandhi, M. G., Parthiban, S., Thummalu, N. and Christy. A. 2015. NDVI: Vegetation change detection using remote sensing and gis – A case study of Vellore District. *Procedia Computer Science*, 57, pp.1199-1210.

Gibbs, H. K., Browns, S., Niles, J. O., and Foley, J. A. 2007. Monitoring and Estimating tropical forest carbon stocks: Making REDD a reality. *Environmental Research Letters*, 2, pp.1-13.

Gislason, P. O., Benediktsson, J. A. and Sveinsson, J. R. 2006. Random Forests for land cover classification. *Pattern Recognition Letters*, 27(4), pp.294-300.

Gizachew, B., Solberg, S., Næsset, E., Gobakken, T., Bollandsås, J., Zahabu, E. and Mauya, E. W. 2016. Mapping and estimating the total living biomass and carbon in low-biomass woodlands using Landsat 8 CDR data. *Carbon balance and management*, 11 (1), 13. doi:10.1186/s13021-016-0055-8.

Govender, M., Chetty, K., Naiken, V. and Bulcock, H. 2008. A comparison of satellite hyperspectral and multispectral remote sensing imagery for improved classification and mapping of vegetation. *Water SA*, 34(2), pp.147-154.

Hardy, C. and Nel, A. 2015. Data and techniques for studying the urban heat island effect in Johannesburg, *The International Archives of Photogrammetry, Remote Sensing and Spatial Information Sciences*, 40(7), pp.203-206.

Hlatshwayo, S. T., Mutanga, O., Lottering, R. T., Kiala, Z. and Ismail, R. 2019. Mapping forest aboveground biomass in the reforested Buffelsdraai landfill site using texture combinations computed from SPOT-6 pan-sharpened imagery. *International Journal of Applied Earth Observation Geoinformation*, 74, pp.65-77.

Immitzer, M., Atzberger, C. and Koukal, T. 2012. Tree Species Classification with Random Forest Using Very High Spatial Resolution 8-Band WorldView-2 Satellite Data. *Remote Sensing*, 4, pp.2661-2693.

Jiménez-Muñoz, J. C., Sobrino, J. A., Skokovi, D., Mattar, C. and Cristóbal, J. 2014. "Land Surface Temperature Retrieval Methods from Landsat-8 Thermal Infrared Sensor Data", *IEEE Geoscience and Remote Sensing Letters*, 11(10), pp.1840-1843.

Kaplan, G., Avdan, U. and Avdan, Z, Y. 2018. Urban Heat Island Analysis Using the Landsat 8 Satellite Data: A Case Study in Skopje, Macedonia. *Proceedings*, 2(358), pp.1-5.

Kerr, J. B. and Fioletov, V.E. 2008. Surface ultraviolet radiation. *Atmosphere-Ocean*, 46 (1), pp.159-184.

Ketterings, Q. M., Coe, R., Noordwijk, Y. and Palm, C. A. 2001. Reducing uncertainty in the use of allometric biomass equations for predicting aboveground tree biomass in mixed secondary forests. *Forest Ecology and Management*, 146, pp.199-209.

Kibert, C. J. 2012. Sustainable Construction: Green Building Design and Delivery. John Wiley and Sons Inc, Hoboken, NJ, USA.

Kim, C., Jeong, J., Kim, R., Son, Y. and Lee, K. H. 2011. Allometric equations and biomass expansion factors of Japanese red pine on the local level. *Landscape Ecology Engineering*, 7, pp.283-289.

Kumar, L. and Mutanga, O. 2017. Remote Sensing of Above-Ground Biomass. *Remote Sensing*, 9, pp.935-942.

Le Maitre, D. C., O'Farrell, P. J. and Reyers, B. 2007. Ecosystems services in South Africa: a research theme that can engage environmental, economic and social scientists in the development of sustainability science? *South African Journal of Science*, 103(9-10), pp.367-376.

Liou, Y. A., Nguyen, A. K. and Li, M. H. 2017. Assessing spatiotemporal eco-environmental vulnerability by Landsat data. *Ecological Indicators*, 80, pp.52-65.

Liu, L. and Zhang, Y. 2011. Urban Heat Island Analysis Using the Landsat TM Data and ASTER Data: A Case Study in Hong Kong. *Remote Sensing*, 3, pp.1535-1552.

Liu, L., Coops, N. C., Aven, N. W. and Pang, Y. 2017. Mapping urban tree species using integrated airborne hyperspectral and LiDAR remote sensing data. *Remote Sensing of Environment*, 200, pp.170-182.

Lu, D. 2005. Aboveground biomass estimation using Landsat TM data in the Brazilian Amazon Basin. *International Journal of Remote Sensing*, 26, pp.2509-2525.

Lu, D. 2006. The potential and challenge of remote sensing-based biomass estimation. *International Journal of Remote Sensing*, 27, pp.1297-1328.

Martin, A.R. and Thomas, S. C. 2011. A Reassessment of Carbon Content in Tropical Trees. PLoS ONE 6(8): e23533. doi:10.1371/journal.pone.0023533.

McFeeters, S. K. 1996. The Use of Normalized Difference Water Index (NDWI) in the Delineation of Open Water Features. *International Journal of Remote Sensing*, 17(7), pp.1425-1432.

McHale, M. R., Burke, I. C., Lefsky, M. A., Peper, P. J. and McPherson, E. G. 2009. Urban forest biomass estimates: is it important to use relationships developed specifically for urban trees? *Urban Ecosystems*, 12, pp.95-113.

Mexia, T., Vieira, J., Príncipe, A., Anjos, A., Silva, P., Lopes, N., Freitas, C., Santos-Reis, M., Correia, O., Branquinhoa, C. and Pinho, P. 2018. Ecosystem services: Urban parks under a magnifying glass. *Environmental Research*, 160, pp.469-478.

Motlagh, M. G., Kafaky, S. B., Mataji, A. and Akhavan, R. 2018. Estimating and mapping forest biomass using regression models and Spot-6 images (case study: Hyrcanian forests of north of Iran). *Environmental Monitoring and Assessment*, 190(6), pp.352-366.

Muhd-Ekhzarizal, M.E., Mohd-Hasmadi, I., Hamdan, O., Mohamad-Roslan, M. K. and Noor-Shaila, S. 2018. Estimation of aboveground biomass in Mangrove forests using vegetation indices from SPOT-5 image. *Journal of Tropical Forest Science* 30(2), pp.224-233.

Mutanga, O. and Skidmore, A. K. 2004b. Narrow band vegetation indices overcome the saturation problem in biomass estimation. *International Journal of Remote Sensing*, 25(19), pp.3999-4014.

Myeong, S., Nowak, D. J. and Duggin, M. J. 2006. A temporal analysis of urban forest carbon storage using remote sensing. *Remote sensing of the environment*, 101, pp.277-282.

Nelson, B. W., Mesquita, R., Pereira, J. L. G., Aquino de Sauza, S. G., Batista, G. T. and Couto, L.B. 1999. Allometric regressions for improved estimate of secondary forest biomass in the Central Amazon. *Forest Ecology and Management*, 117, pp.149-167.

Newete, S. W., Oberprieler, R. G. and Byrne, M. J. 2011. The host range of the Eucalyptus Weevil, Gonipterus "scutellatus" Gyllenhal (Coleoptera: Curculionidae), in South Africa. *Annals of Forest Science*, 68, pp.1005-1013.

Ngo, K. M. and Lum, S. 2018. Aboveground biomass estimation of tropical street trees. *Journal of Urban Ecology*, 4(1), pp.1-6.

Nowak, D. J. 1993. Atmosphere carbon reduction by urban trees. *Journal of Environmental Management*, 37, pp.207-217.

Nowak, D. J., Hoehn, R. E., Crane, D. E., Stevens, J. C. and Walton, J. T. 2007. Assessing Urban Forest Effects and Values: San Francisco's Urban Forest. USDA Forest Service, New York, USA.

Odindi, J., Adam, E., Ngubane, Z., Mutanga, O and Slotow, R. 2014. Comparison between WorldView-2 and SPOT-5 images in mapping the bracken fern using the random forest algorithm. *Journal of Applied Remote Sensing*, 8, pp.1-16.

Ogunode, A. and Akombelwa. 2017. An algorithm to retrieve Land Surface Temperature using Landsat-8 Dataset. *South African Journal of Geomatics*, 6(2), pp.262-276.

Omar, H., Norsheilla, J., Ismail, I., Kassim, A. R. and Musa, S. 2016. '*Combination of PALSAR-2 AND SPOT-6 images for estimating aboveground biomass of Peat swamp Ecosystem in Malaysia'*. Kuching, Sarawak, Malaysia., 15-19 August. Malaysia Peat Society.

Orimoloye, I. R., Mazinyo, S. P., Nel, W. and Kalumba, A. M. 2018. Spatiotemporal monitoring of land surface temperature and estimated radiation using remote sensing: human health. *Environmental Earth Sciences*, 77, pp.1-10.

Pal, S. and Ziaul, S. 2017. Detection of land use and land cover change and land surface temperature in English Bazar urban centre. *The Egyptian Journal of Remote Sensing and Space Sciences*, 20, pp.125-145.

Pal. M. 2005. Random forest classifier for remote sensing classification. *International Journal of Remote Sensing*, 26(1), pp.217-222.

R Core Team. 2016. R: A language and environment for statistical computing. *A Foundation for Statistical Computing*, Vienna, Austria. https://www.R-project.org/ [Accessed 26 January 2019].

Rouse, J. W., Haas, R. H., Schell, J. A. and Deering, D. W. 1974. Monitoring vegetation systems in the Great Plains with ERTS. Freden, S.C., Mercanti, E. P. and

Becker, M. A. (Eds). *Third Earth Resources Technology Satellite-1 Symposium*, Washington D., USA, pp.48-62.

Roy, D. P., Kovalskyy, V, Zhang, H. K, Vermote, E. F, Yan, L., Kumar S. S. and Egorov, A. 2016. Characterization of Landsat-7 to Landsat-8 reflective wavelength and normalized difference vegetation index continuity. *Remote Sensing of Environment*, 185, pp.57-70.

Roy, D. P., Wulder, M. A., Loveland, T. R., Woodcock, C. E., Allen, R. G., Anderson, M. C., Helder, D., Irons, J. R., Johnson, D. M., Kennedy, R., Scambos, T. A., Schaaf, C. B., Schott, J. R., Sheng, Y., Vermote, E. F., Belwardo, A. S., Bindschadler, R., Cohenq, W. B., Gao, F., Hipple, J. D., Hostert, P., Huntington, J., Justice, C. O., Kilic, A., Kovalskyy, V., Lee, Z. P., Lymburner, L., Masek, J. G., McCorkel, J., Shuai, Y., Trezza, R., Vogelmannc, J., Wynne, R. H. and Zhud, Z. 2014. Landsat-8: science and product vision for terrestrial global change research. *Remote Sensing Environment*, 145, pp.154-172.

Schäffler, A. and Swilling, M. 2013. Valuing green infrastructure in an urban environment under pressure- The Johannesburg case. *Ecological Economics*, 86, pp.246-257.

Seburanga, J. L., Kaplin, B. A., Q. X. and Gatesire, T. 2014. Amenity trees and green space structure in urban settlements of Kigali, Rwanda. *Urban Forestry and Urban Greening*, 13, pp.84-93.

Shalaby, A. and Tateishi, R. 2007. Remote sensing and GIS for mapping and monitoring land cover and land-use changes in the North-western coastal zone of Egypt. *Applied Geography*, 27(1), pp.28-41.

Shekhar, S and Kumar, S. 2014. Assessing the quality of urban environment through urban neighbourhood green index. ISPRS TC VIII International Symposium on "Operational Remote Sensing Applications: Opportunities, Progress and Challenges", Hyderabad, India, pp.9-12.

Shojanoori, R., Shafri, H. Z. M., Mansor, S. and Ismail, M. H. 2016. The Use of WorldView-2 Satellite Data in Urban Tree Species Mapping by Object-Based Image Analysis Technique. *SainsMalaysiana*, 45(7), pp.1025-1034.

Sousa, A. M. O., Goncalves, A. C., Mesquita, P. and Marques da Siva, J. R. 2015. Biomass resolution satellite images: A case study of *Quercus rotundifolia*. *Journal of Photogrammetric and Remote Sensing*, 101, pp.169-179.

Sousa, M. O., Gonçalves, A. C., and Marques da Silva, J. R. 2017. Above-Ground Biomass Estimation with High Spatial Resolution Satellite Images, Biomass Volume Estimation and Valorization for Energy. Chapter 3. J. S. Tumuluru (Editor). DOI: 10.5772/65665.

Stathopoulou, M. and Cartalis, C. 2007. "Daytime urban heat islands from Landsat ETM+ and Corine land cover data: An application to major cities in Greece". *Solar Energy*, 81(3), pp.358-368.

Statistics South Africa. http://www.statssa.gov.za/2011 Census. [Accessed 20 November 2018].

Sun, Q., Wu, Z. and Tan, J. 2012. The relationship between land surface temperature and land use/land cover in Guangzhou, China. *Environmental Earth Sciences*, 65, pp. 1687-1694.

Tan, P. Y., Wang, J. and Sia, A. 2013. Perspectives on five decades of the urban greening of Singapore. *Cities*, 32, pp.24-32.

Tietema, T. 1993. Biomass determination of fuel wood trees and bushes of Botswana, Southern Africa. *Forest Ecology and Management*, 60, pp.257-269.

Turton, A., Schultz, C., Buckle, H., Kgomongoe, M., Malungani, T. and Drackner, M. 2006. Gold Scorched Earth and Water: The Hydro politics of Johannesburg. *Water Resources Development*, 22(2), pp.313-335.

United States Geological Survey (USGS). Landsat 8 (L8) Data Users Handbook, LSDS-1574.2016. Version 2.0, URL: https://landsat.usgs.gov/documents/Landsat8 Data Users Handbook.pdf (Accessed 20 November 2018).

Vashum, K. T. and Jayakumar, S. 2012. Methods to Estimate above Ground Biomass and Carbon Stock in Natural Forests- A review. *Journal of Ecosystem and Ecography*, 2(4), pp.1-7.

Wang, D., Wan, B., Qiu, P., Su, Y., Guo, Q., Wang, R., Sun, F. and Wu. X. 2018. Evaluating the Performance of Sentinel-2, Landsat 8 and Pléiades-1 in Mapping Mangrove Extent and Species. *Remote Sensing*, 10, pp.1-27.

Wang, Q. and Tenhunen, J. 2004. Vegetation mapping with multitemporal NDVI in North Eastern China Transect (NECT). *International Journal of Applied Earth Observation Geoinformation*, 6, pp.17-31.

World Health Organization. 2002. Global Solar UV Index: A Practical Guide. Geneva, Switzerland. http://www.who.int/uv/publications/en/UVIGuide.pdf. (Accessed 20/ 02/ 2019).

World Health Organization. 2013. Urban Population Growth. Available: (Accessed 10 April 2018).

World Health Organization. 2016. *Urban green spaces and health.* Copenhagen.

Xie Y., Sha, Z. and Yu, M. 2008. Remote Sensing imagery in vegetation mapping: A review. *Journal of Plant ecology*, 1(1), pp.9-23.

Xie, Y., Sha, Z., Yu, M., Bai, Y. and Zhang, L. 2009. A comparison of two models with Landsat data for estimating above ground grassland biomass in Inner Mongolia, China. *Journal of Ecological modeling*, 220, pp.1810-1818.

Xue, J. and Su, B. 2017. Significant Remote Sensing Vegetation Indices: A Review of Developments and Applications. *Journal of Sensors*, 1, pp.1-17.

Yang, J., Zhao, L., Mcbride, J. and Gong, P. 2009. Can you see green? Assessing the visibility of urban forests in cities. *Landscape and Urban Planning*, 91(2), pp.97-104.

Zhang, Y. 2006. Land surface temperature retrieval from CBERS-02 IRMSS thermal infrared data and its applications in quantitative analysis of urban heat island effect. *Journal of Remote Sensing*, 10, pp.789-797.

Zhao-Liang, L., Hua, W., Ning, W., Qiu, S., Sobrino, J. A., Zhengming, W., Bo-Hui, T. and Guangjian, Y. 2013. Land surface emissivity retrieval from satellite data. *International Journal of Remote Sensing*, 34(9-10), pp.3084-3127.

APPENDICES

FIELD DATA COLLECTION SHEET

SITE……..... DATE……

Tree species	**Latitude**	**Longitude**	**Stem/ trunk Circumference (m)**